POPULAR APPROACHES TO ENGINEERING

Editor: Assoc. Prof. Dr. M. Sait CENGİZ

DUVAR

POPULAR APPROACHES TO ENGINEERING

Editor

Assoc. Prof. Dr. Mehmet Sait CENGİZ

POPULAR APPROACHES TO ENGINEERING
Editor: Assoc. Prof. Dr. Mehmet Sait CENGİZ

Editor in chief: Berkan Balpetek
Cover and Page Design: Duvar Design
Printing : June -2024
Publisher Certificate No: 49837
ISBN: 978-625-6069-32-9

© Duvar Yayınları
853 Sokak No:13 P.10 Kemeraltı-Konak/İzmir
Tel: 0 232 484 88 68

www.duvaryayinlari.com
duvarkitabevi@gmail.com

TABLE OF CONTENTS

Chapter 1

Design Process of Natural and Waste Fiber-Based Exterior Wall Insulation Panels

Aylin ÖZODABAŞ[1]
Nazım Çağatay DEMİRAL[2]

[1] Doç. Dr.; Bilecik Şeyh Edebali Üniversitesi Mühendislik Fakültesi İnşaat Mühendisliği Bölümü. aylin.ozodabas@bilecik.edu.tr ORCID No: 0000-0002-6011-980X

[2] Arş. Gör.; Bilecik Şeyh Edebali Üniversitesi Mühendislik Fakültesi İnşaat Mühendisliği Bölümü. cagatay.demiral@bilecik.edu.tr ORCID No: 0000-0001-5927-7299

Abstract

This research introduces a novel prototype insulation product designed for waterproofing building facades, utilizing a combination of hemp, waste cellulose, and expanded clay. The study aims to offer an alternative to conventional cement-based panels by incorporating plant fibers and waste cellulose.

Hemp was utilized in two forms: fiber and pieces, in varying quantities. Cellulose was employed in both waste and non-waste forms. To reduce their hydrophilicity, both hemp and cellulose fibers underwent pretreatment processes, including boiling, alkali exposure, and paraffin coating. The microstructures of the different fibers were analyzed using SEM. Various tests were conducted to assess strength, density, porosity, and water absorption. The experiments revealed that samples containing hemp and non-waste cellulose exhibited notable dispersion in water absorption tests. The samples with the best performance in terms of strength, water absorption, and porosity were those containing ground expanded clay.

Keywords: Construction Material, Insulation Panel, Natural Fiber, Waste Fiber

1 Introduction

Increasing environmental awareness around the world has greatly influenced materials engineering and design. The growing interest in the use of natural materials addresses ecological issues such as recyclability and environmental safety. Today, synthetic fibers such as glass, carbon and aramid are widely used in polymer-based composites due to their high hardness and strength properties [1]. However, these fibers are associated with biodegradability, initial processing costs, recyclability, energy consumption, machine wear, health hazards, etc. has serious drawbacks [2], [3].

Plastic waste from construction in 2016 was 175 thousand tons, constituting 4.8% of the total [4]. Acoustic absorption panels made from natural fibers are less harmful to human health and more environmentally friendly than those made from traditional synthetic fibers. Although natural fibers have a number of advantages, some of their shortcomings, such as low interfacial adhesion, poor moisture resistance, and low microbial resistance, need to be mitigated for use in effective insulation applications [5].

Nowadays, industries are looking for more durable yet lightweight structural elements. Fiber-cement is a material made from cement, fibers, additives and water, characterized by being light and durable, and used for coating, insulation and waterproofing purposes in construction, especially in lightweight systems [6]. When the literature was examined, it was determined that there was not enough research on the study of fiber cement, and that it was mostly focused on the study of concrete and cement. For this reason, there is a need for alternative studies on fiber cement material by reinforcing it with silica sand, expanded clay and natural fibers. In recent years, a number of experimental studies on hemp, straw, cotton fibers, flax, and wood fibers for thermal insulation have aroused increasing interest from the scientific community and industry. They are characterized by high environmental performance and good hydrothermal behavior in walls [7].

Hemp has good insulating properties, excellent mechanical strength and Young's modulus [8]. Hemp grows in as little as 4 months. In terms of oxygen and paper raw material production, 1 decare of hemp is equivalent to 1.4 decares of forest. There is no need to use pesticides when growing hemp. While hemp can be converted into paper 8 times, wood can be converted 3 times. It attracts great attention due to its basic features such as good thermal insulation, low cost, good mechanical properties and fast growth cycle. Unprocessed natural fiber-based materials cannot be used in green building applications without considering chemical or physical modification [9]. The innermost part of the hemp stems is surrounded by woody fibers known as hurds or shives. The outer layer surrounding the hurds consists of fibers (Figure 1). While synthetic fibers have been studied for almost fifty years, knowledge of natural fibers is still limited and needs to be expanded. The most common binder in hemp-concrete is hydrated lime ($Ca(OH)_2$) [10]. In one study, hemp fibers were processed by sol-gel technique to reduce their hydrophilicity. However, they observed that there was no significant difference between the untreated reference samples in vapor permeability tests [11]. It was observed that as hemp density decreased, its thermal conductivity capacity increased [12].

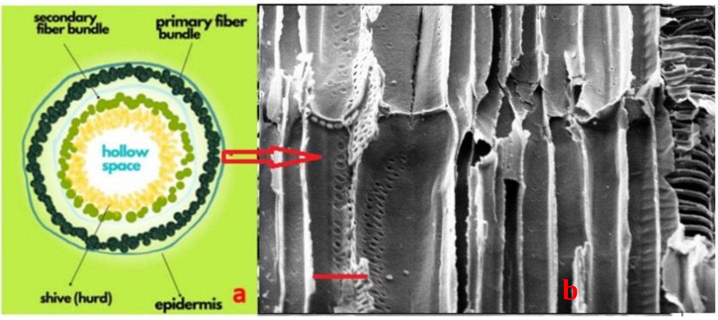

Figure 1. (a) Hemp stem cross-section and
(b) SEM image of hemp cross-section

The strength of natural fibers is significantly lower than glass fibers. But Young's modules are similar values. In addition, the price of natural fiber is approximately 70% lower than glass fiber. Therefore, natural fibers are alternative reinforcing materials for composites because they are readily available, renewable, and cost-effective. Hemp, flax, jute and kenaf fibers are called. They have similar morphologies; cellulose, hemicelluloses and lignin are the main components of fibers [13]. Natural fibers have poor interconnections with the matrix due to their high moisture content. Therefore, the development of surface modifications of the fibers uses alkali concentrations such as NaOH or potassium hydroxide (KOH). This process melts substances such as wax and oil and softens the fiber [14]. Chemical treatments on the fiber can reduce the hydrophilic tendency of the fiber and thus improve compatibility with the matrix [15]. According to another study, the results showed that kenaf fiber which treats with NaOH solution of 6% significantly offered the outstanding performance of the tensile behavior [16]. The alkali treatment removes fiber components, including hemicellulose, lignin, pectin, oil, and wax, revealing cellulose. Thus, it provides enhanced interfacial bonding by increasing the surface roughness. The alkali treatment further transformed the crystalline cellulose into amorphous material. A decrease in moisture uptake has been observed in natural fibers treated with alkali [2]. Fire resistance has also increased as a result of the production of hemp-based materials made hydrophobic with stearic acid. The increased flame retardancy of the samples coated with stearic acid prevented heat transfer to the inner cellulosic fibers by rapidly forming an inorganic protective ceramizing layer on the surface of the hemp fibers during the burning process. Thus, it produced a layer of charcoal and created a physical barrier that could block further combustion [9].

Currently, urea-formaldehyde (UF), phenol-formaldehyde (PF) or melamine-urea-formaldehyde (MUF) adhesives are often involved in the manufacture of chipboard. These types of adhesives have significant disadvantages that pollute the environment and poses a potential carcinogenic risk to workers who manufacture using these adhesives [17]. In some studies, natural adhesives and starch adhesives containing protein and starch have also been used. However, these are often expensive and lead to high production costs [18]. In a study, they observed that the thermal conductivity increased with the increase in the use of both rice straw and mineral wool [19].

The primary innovation and objective of this research is to evaluate the feasibility of producing waterproofing panels for exterior facades utilizing natural or waste materials. Currently, there are limited alternative building materials that can serve as both waterproofing panels and exterior cladding. Although various thermal insulation materials with different compositions and forms exist, waterproofing is predominantly achieved using cement-based fiber-cement products. This reliance on cement-intensive products drives up cement production. Hence, another significant aim of this study is to reduce the cement content while increasing the incorporation of natural or waste fibers. This approach not only aims to enhance the sustainability of the building materials but also seeks to leverage the beneficial properties of alternative fibers to achieve effective waterproofing solutions.

This article consists of three parts; in the first part, the materials and methods of the experiments will be examined. In the second part, the data obtained from the experiments will be represented. In the third and last section, conclusions will be drawn in the light of the data obtained and alternative possible studies will be shed light.

2 Materials and Methods

2.1 Materials

Samples were produced with binary combinations of hemp, waste cellulose, cellulose, expanded clay and granulated expanded clay (GEC) in binary combinations and cement. Waste cellulose was made into pulp by shredding cardboard boxes, which are the waste of the markets, and dried in the oven. Waste cellulose was pulped by shredding cardboard boxes from the waste of the markets and dried in an oven. The expanded clay was ground for 1 hour to below 90 microns.

The fibers subjected pre-treatments, including boiling, sodium hydroxide exposure, and paraffin coating (Figure 3). The fibers were boiled in water for 15 minutes. After boiling, all the fibers absorbed the following certain amounts of water. These absorbed amounts were subtracted from the mixing water. 100g of paraffin was used to coat 25g of fibers. After the paraffin was melted, it was mixed to cover the surfaces of the fibers. In a study, as a pre-treatment, palm fibers were immersed in 5-8% sodium hydroxide (NaOH) solution by weight at room temperature for 2 hours. While the water absorption values in untreated fibers are 8.53%, this value is 4.99% in alkali-treated (5% NaOH) fibers. It has been observed that processed fibers absorb less water. It is understood that the optimum value is 5% NaOH concentration [3]. Pretreatment with NaOH also increased the flexural strength values [20][21]. In another study, defatted fibers were treated with NaOH solution at varying concentrations (2-10%) for 1 hour, then washed several times with distilled water to leach the absorbed alkali and dried. This chemical treatment removed non-cellulosic components and thus improved the quality of the fibers [22] [23]. In Figure 7, hemp images were examined by SEM analysis, and it was seen that smoother images were obtained after treatment. In present study, fibers were kept in 5% NaOH concentration for 3.5 hours. In the preliminary phase of this study samples produced with fibers subjected to three different pre-treatments were tested for water absorption. Among these, the alkali-treated and boiled samples disintegrated during the test. Only the paraffin-coated samples remained solid throughout the water absorption test. Therefore, for the remainder of the study, only paraffin treatment was applied to the fibers to ensure their stability during water exposure.

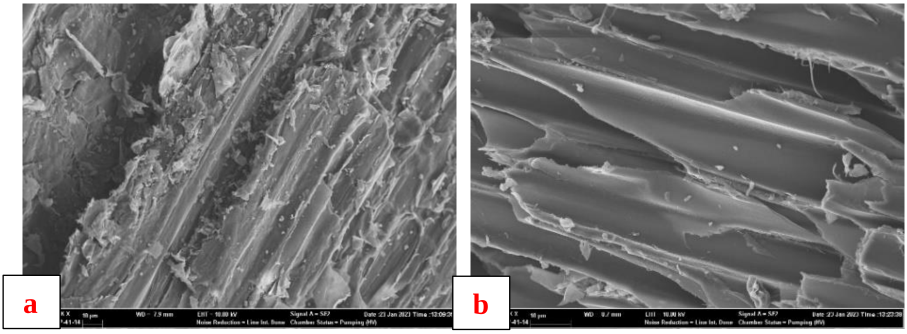

Figure 2. Micrographs of hemp surface a) untreated and b) after NaOH treatment

Figure 4 presents the images of samples from the preliminary phase, illustrating their initial condition. Figure 5 shows the samples fragmented samples when submerged in water or during the production stage, highlighting the stability challenges encountered with certain treatments.

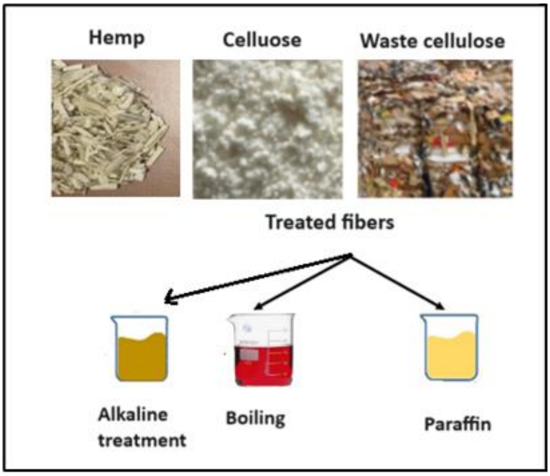

Figure 3. Visual showing the pre-treatments applied to the fibers used in the experimental study

Table 1.Chemical compositions and physical properties of hemp [24]

Chemical compound	**Fibers (%)**
Cellulose	70.2-74.4
Hemicellulose	17.9-22.4
Lignin	3.7-5.7
Pectin	0.9
Fat and wax	0.8
Physical Properties	
Diameter (µm)	8–600
Water absorption (%)	272

Table 2. Mixture ratios of samples containing pretreated fiber and expanded clay (percentage by weight)

Specimens	**Cement**	**Waste cellulose**	**Hemp**	**Cellulose**	**Expanded clay**	**Granulated expanded clay**	**W/B**
WH		10	10	-	-	-	
WC		10	-	10	-	-	
WE		10	-	-	10	-	
WG		10	-	-	-	10	
HC		-	10	10	-	-	
HE		-	10	-	10	-	
HG		-	10	-	-	10	
CE	80	-	-	10	10	-	0.45
CG		-	-	10	-	10	
EG		-	-	-	10	10	
W		20	-	-	-	-	
H		-	20	-	-	-	
C		-	-	20	-	-	
E		-	-	-	20	-	
G		-	-	-	-	20	

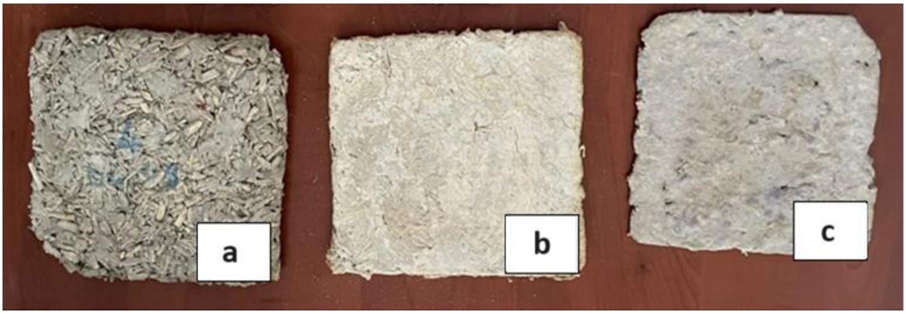

Figure 4. Samples obtained from preliminary experiments. a and b: Specimen containing hemp shive, c: Specimen containing waste cellulose)


Figure 5. Images of samples disintegrated in preliminary experiments

2.2 Preparation of Mortar Samples

Specimens to be tested for strength were placed in 40×40×160 mm steel molds (Figure 6). Samples were produced as plates for water absorption and porosity tests in order to develop products compatible with exterior coating applications produced for waterproofing in the industry. The mixtures in fresh state were poured into 100x100x10 mm molds and pressed by applying a concrete pressure testing machine until a load of 50 kN was reached. The pressed plates were kept in the mold for 24 hours, then removed from the mold and water cured (20±5 °C) until the test day (28 days).

Figure 6. Samples placed in steel molds

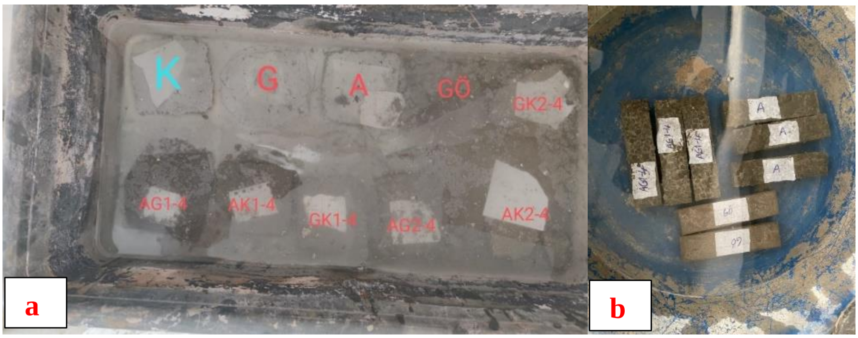

Figure 7. a) Plate-shaped specimens produced to be kept in water and
b) specimens produced to determine strength values

2.3 Method

Among the samples obtained in the first stage, the samples that did not disintegrate during the water absorption test were reproduced and Archimedes and strength tests were carried out.

2.3.1 Strength Tests

Strength tests were carried out based on TSE 196-1 [25] standards (Cement test methods Determination of strength). 7, 14 and 28-day tests were performed on samples kept in the laboratory environment for 28 days.

2.3.2 Water Absorption Test

Water absorption tests were conducted following the TS EN 772-4 [26] standard. The samples were manufactured with dimensions of 15 x 15 x 10 mm and shaped as plates. Each sample was subjected to a pressure of 50 kN.

To evaluate water absorption, the samples were immersed in a water bath at a constant temperature of 20 °C in a laboratory setting for 48 hours. The water content percentage was then calculated using the specified equation.

$$\mathrm{W_c}(\%) = (\mathrm{W_{vc}} - \mathrm{W_{dc}}) * 100/\mathrm{W_{dc}} \tag{2}$$

where W_{wc} is the weight of the water-saturated sample and W_{dc} is the weight of the dry sample.

2.3.4 Density Test

The bulk density Dc is an important indicator of the performance of mortars. For each sample group, the calculation was carried out on a mortar prism sample as follows:

$$Dc = \frac{M_c}{V_c} \tag{3}$$

where M_c is the mass (kg) and V_c is the volume (m^3) of the test sample.

2.3.5 Porosity Test

The porosity determination test was in accordance with TS EN 772-4 [26]. The porosity values of the samples were obtained by using the following equation:

$$\mathrm{P} = \frac{(\mathrm{W_{sat}} - \mathrm{W_{dry}})}{(\mathrm{W_{sat}} - \mathrm{W_{water}})} \times 100 \tag{4}$$

where P is porosity (%), W_{sat} is the saturated surface dry weight of samples (g), W_{dry} is the oven-dried weight of the samples (g), and W_{water} is the weight of samples under water (g).

3 Results

Among the mixtures in Table 2 presented earlier in the materials and methods section, all specimens were disintegrated at the end of water curing except for series W, G, WE, WG and WH, which were treated with paraffin until the day of the experiment. Therefore, only the tests performed on these specimens are presented in this part of the study.

3.1 Flexural and Compressive Test Results

The results of the compressive and flexural tests performed on the samples are presented in Figure 8. The G samples exhibited significantly higher flexural and compressive strength values compared to the other samples. Additionally, the WG samples also demonstrated superior results. This enhancement in strength performance is attributed to the incorporation of GEC in the samples. Thus, the inclusion of GEC substantially improved the mechanical properties of the materials. The milled expanded clay can be considered to provide a homogeneous distribution at the micro level in the panel structure, filling the voids and thus helping the matrix to gain a firmer structure. This may have had a positive effect on the structural integrity and mechanical performance of the panels. Furthermore, the granulated expanded clay can improve stress distribution in the internal structure of the material, preventing the formation of cracks and thus contributing to improved mechanical performance.

The use of organic additives such as hemp and waste cellulose is important in the search for sustainable material solutions; however, in this study, it was observed to have a more pronounced effect on the mechanical properties of granulated expanded clay. These findings could provide a basis for future studies to optimize the use of milled expanded clay and investigate its synergistic effects with other additives.

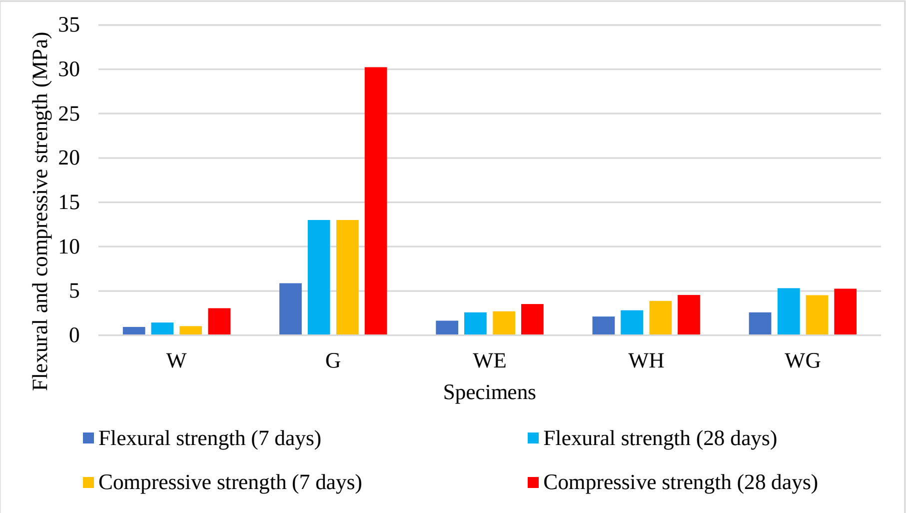

Figure 8. Flexural and compressive strength values of the samples

3.2 Water Absorption Test Results

The best water absorption values were obtained from W and G samples (Figure 9). Waste cellulose was used in sample W, and GEC was used in sample G. It is understood that GEC has a positive effect here, as in the strength values. The highest water absorption value was obtained from WG sample due to the hemp contained in it. Ground expanded clay can reduce the rate of water absorption by making it difficult for water to penetrate into the material. The microstructure of this clay can form a closed-cell structure that prevents the passage of water molecules. Waste cellulose has also been observed to be effective in improving water absorption performance. Cellulose fibres can interlock within the material to form a network structure that prevents the passage of water. Instead of retaining water molecules, these fibres act as an indirect barrier, preventing water from penetrating the internal structure. In the study, the treatment with paraffin during the incorporation of waste cellulose into the mixtures may have made a significant contribution to the improvement in the water absorption performance of this material. Paraffin treatment changes the surface properties of waste cellulose fibres, making it difficult for water to penetrate between the fibres. This process gives the cellulose fibres a hydrophobic character, reducing the absorption of water into the material. Since paraffin is a substance that repels water molecules due to its molecular structure, the resistance of the fibres against water increases as a result of this process. The lower water absorption values of mixtures containing paraffin-treated waste cellulose indicate the effectiveness of this hydrophobic layer. This indicates that cement-based mixtures containing paraffin-treated waste cellulose can be preferred for applications exposed to water, especially for exterior cladding, foundation insulation and other construction materials requiring moisture control. Furthermore, this method also supports sustainable construction practices by contributing to the utilization of waste materials and the development of environmentally friendly building materials.

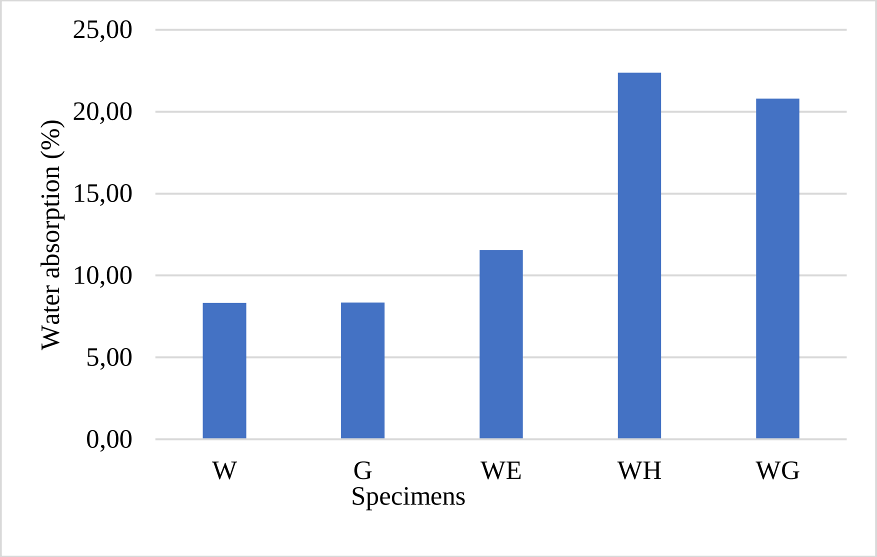

Figure 9. Water absorption values of the samples

3.3 Density Test Results

The highest density value was obtained from the G sample, and the lowest was obtained from the WH sample (Figure 10). The density value of the G sample was obtained as 1.91 g/cm^3. Considering that the average density of concrete panels is 1.30 g/cm^3, it is slightly higher than this value. The fact that it weighs a little more can be seen as a disadvantage. However, if used with a small amount of waste cellulose, the density can be reduced slightly.

3.4 Porosity Test Results

The G sample gave the best porosity values, as in the strength and water absorption tests. The surfaces with the highest porosity yielded samples containing hemp and unground clay (Figure 11). Porosity values also showed similar rates with water absorption. In other words, it is understood that as porosity decreases, water absorption values also decrease (Figure 12). The presence of a strong correlation between water absorption and porosity values in your experimental results, determined by a high regression coefficient of 0.93, shows that these two properties are closely related to each other. This high correlation coefficient indicates that the water absorption capacity increases proportionally with increasing porosity. That is, the higher the porosity of the material, the higher the water absorption capacity.

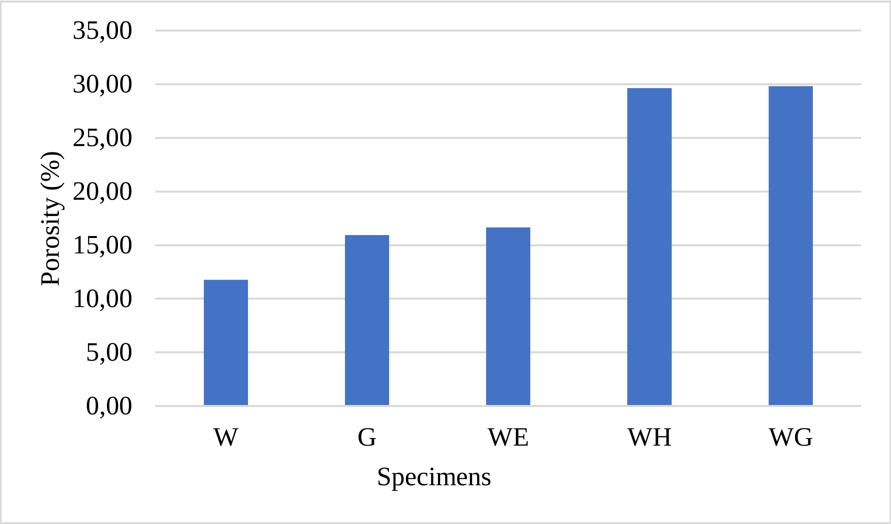

Figure 11. Porosity values of the samples

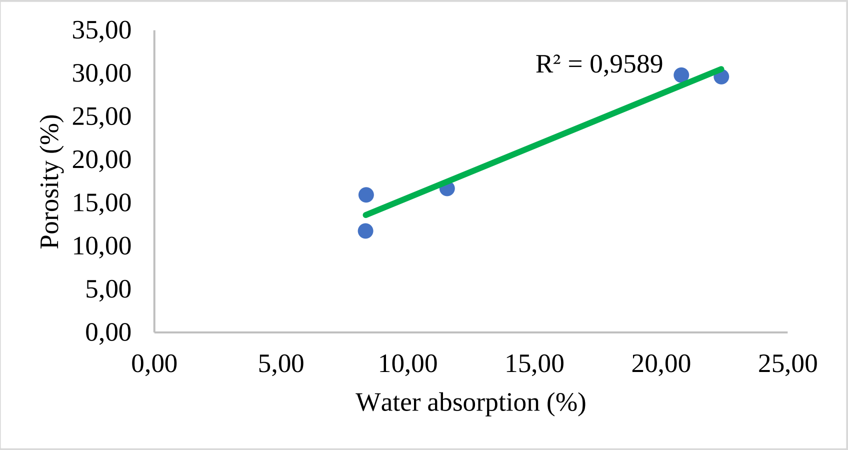

Figure 12. Regression plot showing the linear relationship between porosity and water absorption

4 Conclusion

In conclusion, the investigation presented in this study has explored the potential of integrating natural and waste fibers, particularly hemp and cellulose, with expanded clay to fabricate waterproofing panels for exterior building facades. The research findings underscore the efficacy of this novel composite material in providing sustainable, durable, and effective waterproofing solutions. Here are the key outcomes of the study:

- Considering that the water absorption values of cementitious panels are below approximately 25%, the water absorption values of G samples are considered to be 8%, which can be seen as a very good value. However, since their density is high, their density can be reduced by using small amounts of waste cellulose. Thus, it may be possible to produce water-resistant panels by utilizing waste cellulose and using less cement.
- A strong correlation, with a regression coefficient of 0.96, was observed between water absorption and porosity, highlighting the importance of minimizing porosity to reduce water ingress in waterproofing applications.
- The inclusion of GEC significantly improved the physical and mechanical properties of the composite panels, suggesting its critical role in the overall performance of the waterproofing system. In this case GEC should be used without fiber.
- It is evident from the research findings that the fibers, in their current form and application within the composite, do not significantly enhance the desired properties of the waterproofing panels. However, it is crucial to acknowledge the potential variability in their performance when subjected

to specific environmental factors, such as ultraviolet (UV) radiation and freeze-thaw cycles. These aspects necessitate in-depth exploration in future research to comprehensively understand the fibers' behavior and determine their conclusive effect on the durability and performance of the composite material.

- The study aligns with the principles of sustainable construction by showcasing the potential of utilizing waste and natural fibers to reduce cement usage, thereby contributing to environmental conservation and promoting the development of eco-friendly building materials.
- Economic analysis is also recommended to assess the cost-effectiveness of these innovative materials, determining their viability for commercialization and widespread use in the construction industry.
- These findings provide a solid foundation for further exploration into the use of sustainable materials in construction, offering a promising avenue for the development of environmentally friendly and efficient waterproofing solutions.

5 REFERENCES

[1] K. L. Pickering, M. G. A. Efendy, and T. M. Le, “A review of recent developments in natural fibre composites and their mechanical performance,” Compos. Part A Appl. Sci. Manuf., vol. 83, pp. 98–112, 2016.

[2] M. M. Kabir, H. Wang, K. T. Lau, and F. Cardona, “Chemical treatments on plant-based natural fibre reinforced polymer composites: An overview,” Compos. Part B Eng., vol. 43, no. 7, pp. 2883–2892, 2012.

[3] J. Rout, M. Misra, S. S. Tripathy, S. K. Nayak, and A. K. Mohanty, “The influence of fibre treatment of the performance of coir-polyester composites,” Compos. Sci. Technol., vol. 61, no. 9, pp. 1303–1310, 2001.

[4] J. R. Zhao, R. Zheng, J. Tang, H. J. Sun, and J. Wang, “A mini-review on building insulation materials from perspective of plastic pollution: Current issues and natural fibres as a possible solution,” J. Hazard. Mater., vol. 438, no. February, p. 129449, 2022.

[5] H. Srinivasan et al., “Desert cotton and areca nut husk fibre reinforced hybridized bio-benzoxazine/epoxy bio-composites: Thermal, electrical and acoustic insulation applications,” Constr. Build. Mater., vol. 363, no. November 2022, p. 129870, 2023.

[6] D. M. Gomez Mejia, D. F. Hincapie-Rojas, F. N. Jimenez-Garcia, and C. A. Alvarez Vargas, “Effect of the addition of silica obtained from rice husk on physicochemical and mechanical properties of fibercement,” Heliyon, vol. 9, no. 2, 2023.

[7] F. Mnasri, S. Bahria, M. E. A. Slimani, O. Lahoucine, and M. El Ganaoui, “Building incorporated bio-based materials: Experimental and numerical study,” J. Build. Eng., vol. 28, no. November 2019, p. 101088, 2020.

[8] P. Peças, H. Carvalho, H. Salman, and M. Leite, “Natural fibre composites and their applications: A review,” J. Compos. Sci., vol. 2, no. 4, pp. 1–20, 2018.

[9] G. Viscusi, S. Liparoti, R. Pantani, G. Barra, and G. Gorrasi, “A layer-by-layer approach based on APTES/Cloisite to produce novel and sustainable high performances materials based on hemp fiberboards,” Polym. Degrad. Stab., vol. 198, p. 109892, 2022.

[10] S. Barbhuiya and B. Bhusan Das, “A comprehensive review on the use of hemp in concrete,” Constr. Build. Mater., vol. 341, no. May, p. 127857, 2022.

[11] A. Hussain, J. Calabria-holley, M. Lawrence, and Y. Jiang, “Hygrothermal and mechanical characterisation of novel hemp shiv based thermal insulation composites,” Constr. Build. Mater., vol. 212, pp. 561–568, 2019.

[12] R. Walker and S. Pavía, “Moisture transfer and thermal properties of hemp-lime concretes,” Constr. Build. Mater., vol. 64, pp. 270–276, 2014.
[13] R. Sepe, F. Bollino, L. Boccarusso, and F. Caputo, “Influence of chemical treatments on mechanical properties of hemp fiber reinforced composites,” Compos. Part B Eng., vol. 133, pp. 210–217, 2018.
[14] R. M. Luqman, M. Azlan Suhot, and M. Zaki Hassan, “Effect of alkaline treatment on the single natural fiber strength using Weibull analysis probabilistic model,” Mater. Today Proc., no. xxxx, pp. 1–5, 2023.
[15] K. Stana-kleinschek, V. Ribitsch, M. Sfiligoj-smole, and C. Science, “Correlation of Regenerated Cellulose Fibres Morphology,” Lenzinger Berichte, vol. 82, no. January 2015, pp. 83–95, 2003.
[16] M. I. Ibrahim, M. Z. Hassan, R. Dolah, M. Z. M. Yusoff, and M. S. Salit, “Tensile behaviour for mercerization of single kenaf fiber,” Malaysian J. Fundam. Appl. Sci., vol. 14, no. 4, pp. 437–439, 2018.
[17] D. Cavallo et al., “New formaldehyde-free adhesives for wood manufacturing: In vitro evaluation of potential toxicity of fine dust collected during wood sawing using a new experimental model to simulate occupational inhalation exposure,” Toxicology, vol. 466, no. October 2021, p. 153085, 2022.
[18] J. Shi et al., “Eco-friendly and special-shaped bamboo binderless fiberboards fabricated by self-bonding technology: Effect of bamboo fibers with different sizes,” Ind. Crops Prod., vol. 194, no. October 2022, p. 116300, 2023.
[19] P. O. Awoyera, A. D. Akinrinade, A. G. de Sousa Galdino, F. Althoey, M. S. Kirgiz, and B. A. Tayeh, “Thermal insulation and mechanical characteristics of cement mortar reinforced with mineral wool and rice straw fibers,” J. Build. Eng., vol. 53, no. January, 2022.
[20] A. M. Radzi, S. M. Sapuan, M. Jawaid, and M. R. Mansor, “Effect of Alkaline Treatment on Mechanical, Physical and Thermal Properties of Roselle/Sugar Palm Fiber Reinforced Thermoplastic Polyurethane Hybrid Composites,” Fibers Polym., vol. 20, no. 4, pp. 847–855, 2019.
[21] G. W. Beckermann and K. L. Pickering, “Engineering and evaluation of hemp fibre reinforced polypropylene composites: Fibre treatment and matrix modification,” Compos. Part A Appl. Sci. Manuf., vol. 39, no. 6, pp. 979–988, 2008.
[22] L. Y. Mwaikambo and M. P. Ansell, “Chemical modification of hemp, sisal, jute, and kapok fibers by alkalization,” J. Appl. Polym. Sci., vol. 84, no. 12, pp. 2222–2234, 2002.

[23] A. Santoni et al., “Improving the sound absorption performance of sustainable thermal insulation materials: Natural hemp fibres,” Appl. Acoust., vol. 150, pp. 279–289, 2019.
[24] A. K. Mohanty, M. Misra, and G. Hinrichsen, “Biofibres, biodegradable polymers and biocomposites: An overview,” Macromol. Mater. Eng., vol. 276–277, pp. 1–24, 2000.
[25] TS EN 196-1, Methods of testing cement - Part 1: Determination of strength. 2016, TSE, Ankara-Turkey
[26] TS EN 772-1, Methods of test for masonry units - Part 4: Determination of real and bulk density and of total and open porosity for natural stone masonry units 2002. TSE, Ankara-Turkey

Chapter 2

Adaptive Neuro Fuzzy Inference Systems (ANFIS) and Application to Wear Prediction of Porcelain Ceramics

Tahsin BOYRAZ[1]

[1] Sivas Cumhuriyet University, Metallurgical and Materials Engineering, Sivas, Turkey
tahsinboyraz@cumhuriyet.edu.tr ORCID No: 0000-0003-4404-6388

Abstract

In this study, we investigated the manufacturing characteristics and wear characteristics of porcelain-ceramics-ceramics composites made by powder metallurgy and added aluminium titanate and mullite, and investigated artificial neural network modelling based on the obtained experimental data. Aluminium titanate and mullite ceramic powders prepared from Al_2O_3, SiO_2, and TiO_2 powders by reactive sintering were added to the porcelain powder in different amounts (0 and 20 wt%). Blends prepared by mechanical alloying in an alumina ball mill were prepared by forming in a dry press and then sintering under normal atmospheric conditions. Subsequently, a characterization study of the sintered samples was carried out, and the obtained wear test results were converted into data suitable for modelling by artificial neural networks. In the further course of the research, the experimental wear results were analysed and modelled using artificial neural networks. Wear load, wear time, sintering temperature, and sintering time data were used as input variables for the artificial neural network. The wear value was taken as the output variables of the artificial neural network. Using ANFIS (Adaptive Neuro Fuzzy Inference Systems) learning technique, an artificial neural network was established to predict the wear properties of porcelain-ceramic composites reinforced with mullite and aluminium titanate. As a result, the training and testing results were compared with the real values to control the performance of the network. After the ANFIS estimation, confirmation tests were performed to confirm the experimental results. The highest R^2 values were calculated as 0.9785 in aluminium titanate and mullite doped porcelain.

Keywords: Ceramic, Porcelain, Wear, Artificial Neural Networks, ANFIS.

INTRODUCTION

Porcelain is a hard, durable and compressed clay material. Porcelain is formed by firing at high temperatures and has a thin, glass-like surface. Porcelain is usually white in colour, but can also be found in different colours and patterns. Porcelain is a durable and hard material. It is also water-resistant and hygienic, so it is often used in products such as dinnerware, pottery and bathroom accessories. Porcelain is also resistant to high temperatures, so it can also be used in places with high temperatures, such as ovens and stoves. Porcelain can be classified into two main types: soft porcelain and hard porcelain. Soft porcelain is less compressible and less durable. However, hard porcelain is more compressible and more durable. Porcelain is used in many different areas. In the kitchen, it is used as dinnerware, plates, crockery and other dining utensils. It is also used in bathrooms, sinks and toilets. Porcelain also has decorative uses such as various ornaments, figurines, vases and sculptures. Porcelain is a hard, non-porous, fine-grained, mostly translucent vitrified white ceramic with a quartz, kaolin, and feldspar structure that is fired at high temperatures (Boyraz and Akkuş, 2019,2021; Marquez et.al., 2008, 2009).

Aluminium titanate (Al2O3.TiO2) has fabulous warm stun resistance, moo warm conductivity, moo coefficient of warm extension, and chemical resistance in liquid metal. Used in applications in the ceramic, glass, automotive, and heat treatment industries (Saclı et.al.,2015; Kucuk et.al., 2018; Ozsoy et.al., 2015; Çıtak et.al., 2014; Önen etal., 2014). Aluminium titanate ceramic refractories are one of the prominent material options, especially in severe thermal shock applications. Today, Aluminium titanate ceramics are used especially as thermal insulation filler and diesel particle filter. It is also used in industry, in nozzle manufacturing, foundry and non-ferrous casting industry (Jiang et al. 2011). Because of its low toughness and relatively low strength compared to other ceramics, mullite has never been considered as a material with high strength at low temperatures. However, for high temperature applications, it has long been recognized as a material with excellent creep and thermal shock resistance. In addition, it maintains its strength value at room temperature up to 1560 °C. Because of this feature and the fact that it does not have oxidation problems at high temperatures, mullite is one of the best ceramic materials that can be used both as a single phase and matrix material at high temperatures compared to other ceramics. It was understood that mullite has a very high creep strength, and in the test performed at 900 MPa and 1500 °C, single crystal mullite showed no deformation. The compressive strength of mullite is twice that of alumina at 1400 °C and the same as silicon carbide at 1500 °C. It has 10 times more creep strength at 1450 °C than pure mullite alumina (Hillig,1993). Hillig suggested that the change in hardness depending on temperature could provide information about the high temperature strength of a material. If the hardness does not change with temperature, the mechanical properties of that material are not affected by temperature. Mullite is the material whose hardness decreases the least with temperature, and it has the same hardness as silicon carbide, which is one of the ceramics with the highest hardness over 1000 °C. The reason why the hardness of mullite does not change much with temperature is attributed to the lack of slip systems and thus the dislocations remaining immobile under test conditions (Hillig, 1993; Aksaf, 1983). Mullite is a uniquely stable inter crystalline phase of the binary system Al_2O_3-SiO_2. Mullite ($3Al_2O_3.2SiO_2$) is a good and cheap refractory ceramic. Mullite ceramics have several desirable features, including outstanding thermal and chemical stability, great high temperature strength and flow resistance, and extremely good thermomechanical properties, making them an excellent choice for structural design materials. The coefficient of thermal expansion is relatively small, which ensures good thermal shock resistance (Lee and Iqbal, 2001; Chargui et. al., 2018; Serra et. al., 2016). Ceramic substances have excessive hardness, low friction, exceptional corrosion resistance and the capacity to paintings beneathneath intense situations together with excessive temperatures. Ceramic put on is anisotropic and associated with the crystal shape like metals (Buckley and Miyoshi, 1984; Kong et. al., 1998; Baudín et. al., 2014).

Artificial Neural Networks (ANN) can help reduce the cost of experimentation if done with care and sufficient expertise. Artificial neural networks can be characterized as highly parallelized distributed processors with a characteristic tendency to collect experimental information and make it accessible and usable (Lin Ye et.al., 2005; Koker et.al., 2007). The Artificial Neural Network technique is suitable when a large database is accessible, when it is difficult to find a definitive answer to a problem by scientific methods, and when the information set is insufficient, noisy and complex (Jiang et.al., 2007). Artificial neural networks technique has the opportunity to be applied in many fields, from education to health, from social sciences to science. Similarly, engineering and materials science applications are also increasing rapidly. Thickness, porosity, hardness, strength, wear, stress, etc. of materials. It can predict features such as with reasonable precision (Hassan et.al., 2009; Huang et.al., 2002; Basheer et.al.,2008; Mandal et.al., 2009).

Adaptive Neuro-Fuzzy Inference System (ANFIS) is a machine learning model that incorporates a combination of neural networks and fuzzy logic. ANFIS uses the ability of neural networks to automatically extract and optimize fuzzy rules (Zadeh, 1965; Jang, 1995). This model is used to learn the relationships between input data and output, and is particularly well suited for modelling complex non-linear relationships. ANFIS represents the input variables in fuzzy sets and then uses a set of rules and inference mechanisms to determine the output by activating and combining these sets. ANFIS optimizes these parameters based on the training data, typically using gradient descent or other optimization methods. Application areas of AFIS include prediction, classification, verification, and system identification (Karaboğa and Kaya, 2019). This model can be a powerful tool for modelling and controlling non-complex systems, but it may not be suitable for large and high-dimensional data sets.

In this study, the wear behaviour of aluminium titanate and mullite added porcelain ceramics produced by traditional powder metallurgy method was examined. Experimental data obtained as a result of wear tests were analysed using a machine learning method. Adaptive Neural Fuzzy Inference System (ANFIS) was used to predict the wear behaviour of porcelain ceramics using MATLAB's neural network tool panel. The results were evaluated using statistical measures such as R^2, RMSE, MAE, and MAPE. The models were analysed in terms of their training time, accuracy, and overall fit to the data, showcasing their performance and capabilities.

MATERIALS AND METHODS

Researchers sometimes face challenges in setting up and conducting physical measurements in experimental studies, leading to incomplete data collection. In such cases, simulated data can help bridge the gap. Machine learning algorithms play a key role in predicting outcomes on untested data based on patterns learned from experimental data. The Adaptive Neural Fuzzy Inference System approach has proven successful in generating simulation results by incorporating key aspects of machine learning theories. Experimental models face challenges related to setup times, expenses, and material-device management, impacting workflow. Simulation environments can improve accuracy using statistical or mathematical models to support the system. Artificial Neural Network algorithms excel in modelling system patterns by training on data or past models.

Materials production

This study looked at the wear characteristics of porcelain ceramics with mullite and aluminium titanate added, made using the powder metallurgy process. The experimental wear data were then analysed and artificial neural networks were used to model the results. Using a mechanical alloying process, the mixtures were made uniformly moist in an acetone atmosphere in alumina ball mills. Samples were created by pressing and drying the prepared mixes before they were fired. Reaction sintering was used to create aluminium titanate and Mullite ceramic powders from Al_2O_3, SiO_2, and TiO_2 powders at 1550 oC and 1400 ^oC for two hours, respectively. The powders of mullite and aluminium titanate were prepared for usage by crushing, grinding, and sifting. Different weight percentages (0 and 20 wt%) of AT and M were combined with porcelain (P). Powder metallurgy was used to prepare the porcelain ceramics AT and M strengthened with reinforcement. The combination powders were compressed using uniaxial pressing at 200 MPa to create preforms measuring 56 x 12 x 10 mm. The green compacts were sintered in a high temperature furnace (Protherm^{TM} Furnace) at 1100–1200 ^oC for 1–5 hours while being heated at a rate of 5 oC min–1. Ceramics were put through wear tests using an abrasion tester of the Plint brand. Wear discs are made of steel. Every sample underwent wear testing with force levels of 70, 90, and 120 N for wear durations of 5, 10, 15, and 20 minutes. The specimen was first measured using a 0.0001 g precision scale, and the quantity of wear was ascertained by measuring once more after the designated wear time (Boyraz and Akkuş, 2019,2021). Following that, the sintered samples were characterized, and the wear experiment findings were transformed into data that could be used with the Adaptive Neural Fuzzy Inference System (ANFIS) for modelling.

Fuzzy Logic, Neural Networks and ANFIS

Adaptive Neuro Fuzzy Inference Systems is a structure that combines the learning capacity of neural networks and the uncertainty management capabilities of fuzzy logic. This system optimizes fuzzy rules by learning from training data and thus provides high accuracy in modelling nonlinear systems. ANFIS is widely used, especially in prediction, classification and control systems Jang, 1993; Lin and Lee, 1996; Takagi and Sugeno, 1985). Adaptive Neuro Fuzzy Inference Systems uses ANN and fuzzy logic systems by separating them with certain roles. While ANN is used for learning from data and parameter optimization, fuzzy logic systems are used to work with uncertain and fuzzy information. This structure combines the powerful learning capabilities of ANN with the human-like decision-making processes of fuzzy logic. However, both methods have some limitations on their own. While ANN requires large data sets and may have difficulty learning complex structures, fuzzy logic requires user intervention in manually determining and adjusting the rules. ANFIS combines the strengths of these two methods, creating a model that is adaptive and able to deal with uncertainty (Zadeh, 2021; Karaboga and Kaya, 2022).

Fuzzy Logic is a mathematical framework proposed by Zadeh in 1965 that can process information containing uncertainty and fuzziness by expanding the binary (0 and 1) structure of classical logic. Its basic structure works similar to human thought and decision-making processes, allowing modeling imprecise data and linguistic expressions. This structure is built on fuzzy set theory and determines the degree to which elements are in a certain set through membership functions. Fuzzy rules and inference mechanisms are the basic components of fuzzy logic, and these rules are expressed in the form of "If-Then". The main purpose of the model is to transform ambiguous and incomplete information into meaningful and usable results. Fuzzy logic is widely used in control systems, decision support systems, and various engineering applications, because its capacity to deal with uncertainty and its flexible structure offer great advantages in the management of complex systems (Zadeh,2021; Mendel and John, 2020).

Artificial intelligence (AI) is a branch of technology that enables machines to develop capabilities similar to human intelligence. The theoretical basis of Artificial intelligence is based on algorithms that mimic the functioning of the human brain. These machines are capable of carrying out tasks like learning, reasoning, solving problems, perceiving, and comprehending language that call for human intellect. Artificial intelligence has sub-branches such as machine learning and deep learning. Machine learning uses algorithms that have the ability to learn from data, allowing models to be trained to perform specific tasks. Deep learning, on the other hand, extracts and learns features from complex data structures using multi-layer artificial neural networks. The difference between Artificial intelligence and other machine learning methods is that it has a more general scope and offers a wider range of applications by using different techniques (such as machine learning, natural language processing, computer vision). Artificial intelligence architecture generally consists of data collection, data pre-processing, model training, and model evaluation phases. This architecture enables the development of customized solutions in various industries (healthcare, finance, automotive, etc.) (Russell and Norvig, 2020; Chollet, 2018).

The key factor of neuro fuzzy logic is that it combines the learning ability and associated structures of ANNs with the ease of making human-like decisions and providing expert knowledge. In this way, while fuzzy logic systems are given the learning and calculation power of ANNs, fuzzy control and expert knowledge providing capabilities are added to ANNs. The neuro-fuzzy control system determines the values of the variables that will form its structure by using ANN and fuzzy logic techniques. There are two types of tuning in fuzzy logic controllers: structural and variable tuning. Structural tuning includes fuzzy logic rule structures such as the number of variables to be calculated, the number of rules, and the partitioning of domains of input and output variables. Once the appropriate rule structure is obtained, controller variables need to be set. At this stage, the appropriate centers, slopes, widths and weights of the rules of the membership functions are calculated (Yüksek, 2007).

Neural Fuzzy Logic Networks

Neural Fuzzy Network Structures basically consist of two structures. In the first structure (Figure 1), fuzzy inference; The outputs created according to linguistic expressions are given as input vectors to the multilayer neural network. In this structure, the neural network is trained and the desired outputs are provided. In the second neural fuzzy logic structure (Figure 2), the outputs of the multilayer neural network drive the fuzzy inference mechanism.

Although the rules created from expert knowledge in the fuzzy logic approach can be labelled with linguistic expressions, generally design; It takes a long time because it is done by trial and error method. These rules can be created using neural networks. In the neural fuzzy logic approach, neural networks are used to adapt the membership functions of the decision-making mechanism of fuzzy logic systems.

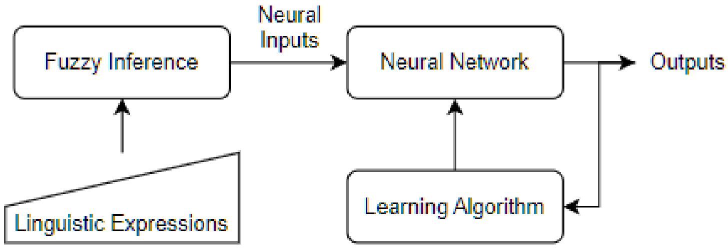

Figure 1: First structure of neural fuzzy logic system

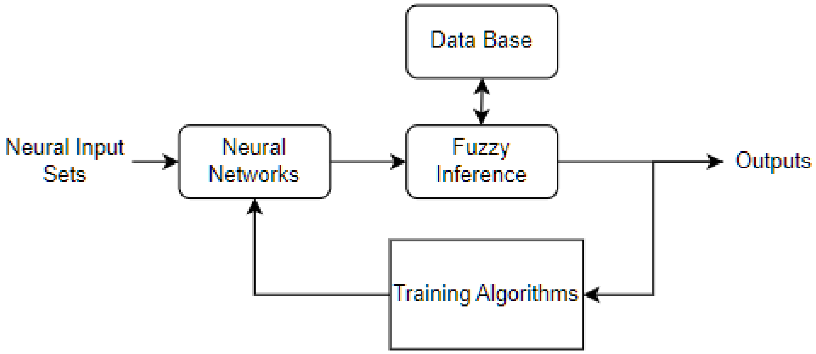

Figure 2: Second structure of neural fuzzy logic system

ANFIS (Adaptive Network Based Fuzzy Inference System)

ANFIS architecture consists of the representation of Sugeno type fuzzy logic systems as a network model with neural learning capability. This network structure consists of nodes placed in different layers, each of which undertakes the task of performing a defined function (Tsoukalas and Uhrig, 1996).

Let us assume that the fuzzy inference system has one output (z) and two inputs (x and y). A first-order Sugeno fuzzy model with two fuzzy if-then rules typically has the following rule form:

Rule-1 If x is A1 and y is B1, then $f_1 = p_1 x + q_1 y + r_1$

Rule-2 If x is A2 and y is B2, then $f_2 = p_2 x + q_2 y + r_2$

It is shown as Figure 3 shows the reasoning mechanism for this Sugeno fuzzy model. The graphic of the equivalent ANFIS architecture representing this structure is shown in Figure 4. For this ANFIS architecture in question, nodes in the same layer have the same node functions as shown below. (Here it is stated as the output of node i in Layer I.)

LAYER I: Each node i in this layer is an adaptive node whose output is defined as in Equation 1,

$O_{i,j} = \mu A_i(x), i = 1,2,$ or (1)

$O_{i,j} = \mu B_{i-2}(x), i = 3,4,$ for

where x (or y) refers to the entry of the node and Ai (or Bi-2) refers to the fuzzy set of the node in question.

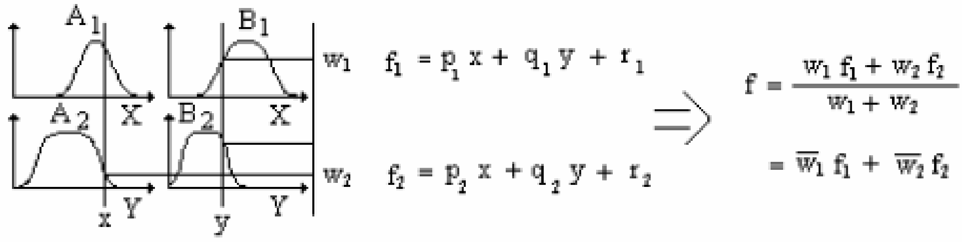

Figure 3: First Order Sugeno Fuzzy Model with Two Inputs and Two Rules

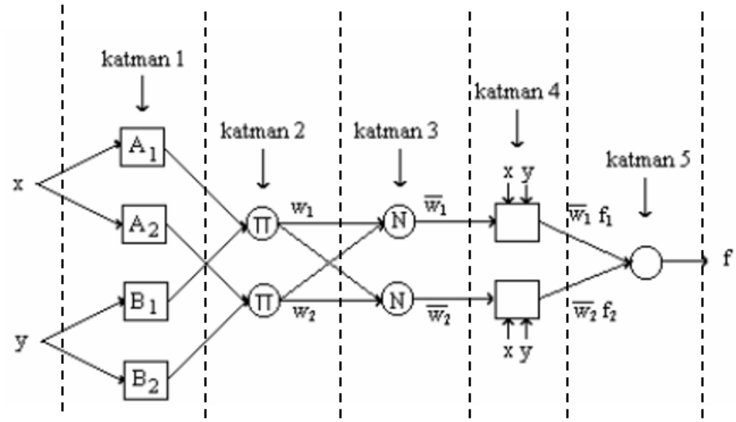

Figure 4. Equivalent ANFIS Structure

In other words, the outputs of this layer create the membership values of the conditional or premise parts of the rules. Here there may be a membership function for Ai and Bi. For example, Ai can be expressed with the generalized bell curve function specified in Equation 2.

$$\mu_A = \frac{1}{1+\left[\left(\frac{x-c_i}{a_i}\right)^2\right]^{bi}} \tag{2}$$

The set {ai, bi, ci} here is the parameter set. The parameters of this layer are referred to as condition or input parameters.

LAYER II: Each node in the second layer is a fixed node labeled with that produces the product of the incoming signals as output. For example;

$$O_{2,i} = w_i = \mu_{Ai}(x)x\mu_{Bi}(y), i = 1,2. \tag{3}$$

Each node's output determines how well each rule is implemented. Knot functions can also be derived from other T-norm operations that carry out the fuzzy (and) operation rather than multiplication in Equation 3.

LAYER III: Each node in the third layer is a fixed node, labelled N. In layer i. knot, i. Calculates the ratio of the execution degree of the rule to the sum of the execution degrees of all rules.

$$O_{3,i} = \overline{w}_i = \frac{w_i}{w_1 + w_2} = 1,2. \tag{4}$$

The outputs of the nodes in this layer are called normalized realization degrees, in accordance with their calculations.

LAYER IV: Each node i belonging to this layer is an adaptive node whose node function is as follows.

$$O_{4,i} = \overline{w}_i f_i = \overline{w}_i (p_i x + q_{iy} + r_i) \tag{5}$$

Here is the output of layer 3 and is the parameter set consisting of the parameters of the nodes in this layer. The parameters of this layer will be expressed as result or output parameters.

LAYER V: In this last layer, there is a single, fixed node, labelled, which collects all incoming signals to calculate the total output.

$$O_{5,i} = Toplam \quad Çıkış = \sum_i \overline{w}_i f_i = \frac{\sum_i w_i f_i}{\sum_i w_i} \tag{6}$$

Thus, an adaptive network structure that fully functions as the Sugeno fuzzy model is built (Jang 1993). ANFIS processing algorithms begin with loading input and output data and initializing ANFIS parameters. During the training phase, membership functions and initial rules are determined. During the training cycle, in the forward pass phase for each training example, the input values are applied to the membership functions, the firing strengths of the rules are calculated and normalized. Output values are calculated and the error between the actual output and the predicted output is found. In the backpass phase, errors are propagated by backpropagation and the parameters are updated. Once training is complete, the model is evaluated using test data and its accuracy is measured. The results are reported and the final parameters of the model are recorded. These processing algorithms enable modelling of complex systems using the learning and adaptation capabilities of ANFIS.

DESIGN OF THE MODEL AND EXPERIMENTAL RESULTS

Data Set Preparation and Experimental System and Data Collection

In this study, time- and load-dependent wear results were performed on porcelain test materials using ANFIS, and the results of these tests, which were not available for similar studies, were modelled. All the data in this study were collected from this article (Tahsin Boyraz and Ahmet Akkuş, Investigation of wear and tear parcels of mullite and aluminium titanate added demitasse pottery, Journal of Ceramic Processing Research, 2021, 22(2), 226- 231). 108 data created from sintering time, sintering temperature, wear time and wear load variables were used in this modelling. These data were then made suitable for machine learning and organized.

Machine learning algorithms discover and learn patterns in data and build mathematical models to predict future data. ML models are directly dependent on the quality of the input data (the defining power of the data set on the model) and its ability to represent the problem in order to produce accurate results. As the data changes over time, more precisely, as the data set for the problem that the ML model provides a solution to develops, studies should be carried out to continuously detect, correct and reduce the problems to increase the accuracy and performance of the model. In short, the model may need to be retrained with the latest data. It has a profound impact on the success of data optimization analysis in machine learning models. Machine learning modelling has four main processes for analysing complex data: problem identification, data curation, neural network modelling, and data analysis. In the first process, problem definitions and expected outcomes are formulated to guide subsequent tasks. The purpose of the alternative process is to prepare high quality data for data analysis to obtain satisfactory results. In the third process, neural network models are iteratively trained after initialization.

As a result, the goal of complex data analysis similar to data mining and decision support can be achieved based on the generalized results (Yu et.al., 2006). The parameters that make up the dataset used to train the ANFIS model in this study are shown in Figure 5.

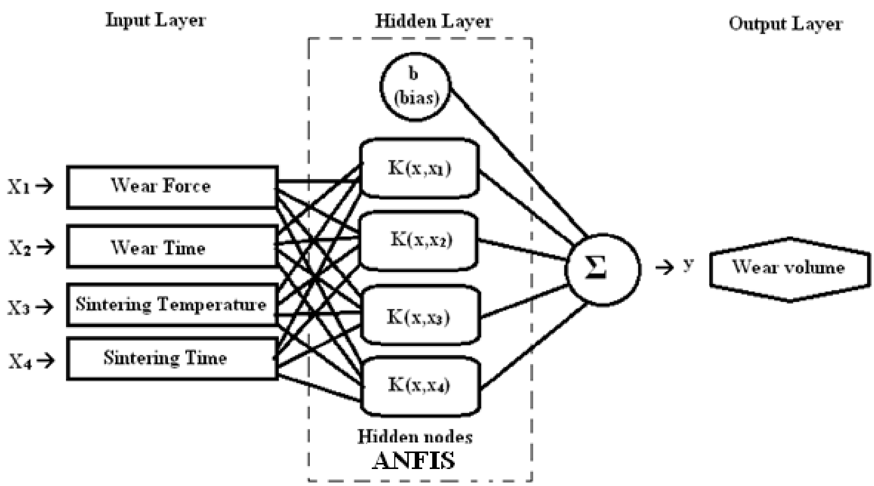

Figure 5: Structure of the created ANFIS model

Setting the ANFIS Model

With the proposed model, the values given as input and output parameters to the system will be tried to be estimated. The ANFIS model will be designed to produce this decision output at acceptable values. The data set to be used in the training of the ANFIS learning model is divided into three parts as “Training Set 70%”, Test Set 15%” and “Confirmation Set 15%”. This separation process was carried out in such a way that the records in the data set were "RANDOM" at the determined rates. While the "Training and Validation" sets were used to train the model, the "Test" set was not presented to the model at any stage of the training. It was used to test the validity and success of the developed model after the training process was completed.

While developing ML models, data set normalization or standardization is a method used especially in statistical data processing areas of computer science such as data mining. The purpose of the method is to deal with the data in a single order in cases where the difference between the data is too great. Another use is to compare data in different scaling systems with each other. The aim here is to carry the data in different systems to a common system and make them comparable by using mathematical functions. Editing the dataset is one of the most important steps. In this study, these methods were not applied on the structure of the data set and all data were used even though they were originally measured.

The steps of training the ANFIS model to determine its parameters are as shown in Figure 6. ANFIS applies two techniques to update parameters. ANFIS uses the gradient descent method to fine-tune the antecedent parameters that define the membership functions, and the least squares method for consecutive parameters that define the coefficients of each output equation. This approach is called hybrid learning method because it combines gradient descent and least squares method, and this method was also used in this study.

The structure of ANFIS contains 5 layers (fuzzy, rule, normalization, defuzzification, output collection node). It uses a fuzzy iteration system during the ANFIS training and evaluation process. The ANFIS framework creates the first fuzzy inference system (FIS) based on the training data. The FIS generated in this way is trained to minimize errors in the output values. Training is done with the strengthening function. The most important parameters to define when creating a FIS are the number of rules to define for each ANFIS input parameter and the membership function of those input parameters. In fuzzy set theory, the membership function assigns the degree of precision (TRUE or FALSE, partial precision instead of 0 or 1) to a precise value between 0 and 1. This helps to design systems where reality has uncertainty or ill-defined problems. world problems A membership function is a function that returns a degree of membership of how a given value maps to an input space called the universe of discourse. Each membership function contains a curve representing each point in the specified input section. Depending on the shape of the curve, each membership function is given a special name, i.e. triangular, bell, trapezoidal and Gaussian membership function. There are eight different types of commonly used membership functions (Yüksek et.al., 2015). The functions related to the ANFIS model are implemented through the MATLAB program, and there are six widely used membership functions (Table 1) (Talpur et.al., 2017).

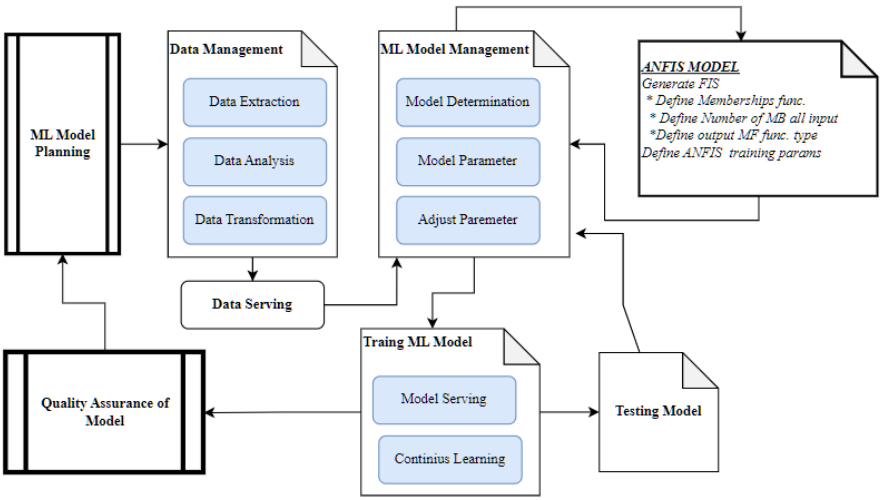

Figure 6: Basic ML and ANFIS Calculation Flow Chart

Table 1: MATLAB Defined Membership Functions

Membership Type	Description
'gbellmf'	Generalized bell-shaped membership function
'trimf'	Triangular membership function
'trapmf'	Trapezoidal membership function
'gaussmf'	Gaussian membership function
'dsigmf'	Difference between two sigmoidal membership functions
'pimf'	Pi-shaped membership function

In order for the ANFIS model to best represent the pattern structure of the data set on which it is trained, the membership functions of the input parameters should be chosen to reflect the effects of the input data on the model. For this reason, by taking the combinations of eight different membership functions to produce the desired results for four inputs, the ANFIS model was trained over approximately 625 different selections and the structure that produced the best output for the model was determined. By using membership functions applied to the inputs of the model with different combinations, the model is trained and statistical value measurement units (Mean Absolute Error (MAE), Root Mean Squared Error (RMSE), Mean Absolute Error (MAE), R Squared (R^2)) are used to test the outputs of the model. The combination of membership functions with the best representative power was determined among the values produced (Table 2a-d). Here, the properties are referenced to the values produced by the data set, which was created from the records selected as random from 15% of the whole data set, initially as the "Test Data Set". Because these set values were not used at any stage of the model during the development and training of the model. Model selection was made based on the R Squared (R^2) values produced by the models produced using different membership functions. Here, the R Squared (R^2) values of the outputs produced by the ANFIS model were ranked using the Test Data Set, Validation Data Set, Whole Data Set and Training Data Set ordering, and the most appropriate model and was selected.

In the ANFIS model training process, the model that produces the best values according to the statistical specification criteria was selected by the results obtained by the different membership functions of the inputs. Table 2a shows the results of the ANFIS model with statistical values for Porcelain (P). According to these results, when the graphic and produced numerical values of the R^2 value, which is the basic indicator, are examined, it is seen that the model succeeds in representing the real system. While establishing ANFIS, the training dataset was divided into 3 parts (Training, Testing and Validation). On the values produced in Table 2a, a high R^2 value of 0.9705 was achieved based on the approach of comparing the success of the model with the TEST data set and the result produced. In the graph given in the table, the distribution agreement between the actual and model data is clearly seen.

Similarly, results were produced for other models. 0.9453 for Porcelain-Mullite (PM) (Table 2b.), 0.9447 (Table 2c.) for Porcelain-Aluminium Titanate (PAT) and 0.9785 for Porcelain-Mullite-Aluminium Titanate (PMAT) (Table 2d.) R^2 values were found. The success of the model can also be seen from the calculated values of other statistical indicators. As shown in the figures in the tables, the distributions of R^2 values and the correlations of the actual calculated values support the ultimate success of the model (González-Sopeña et.al., 2021).

Table 2a: Statistical Scores (P) by Selected Membership Functions

Inputs	X_1	X_2	X_3	X_4
MF	'trimf'	'gbellmf'	'trimf'	'trimf'
	Data Set	Training	Test	Validation
MAPE	0.0703	0.06497	0.0759	0.0860
MAE	0.8707	0.84456	0.8388	1.0075
RMSE	1.1356	1.11266	1.0834	1.2697
R^2	0.9752	0.9784	0.9705	0.9702

Training Dataset Measured and ANFIS-Generated Values

Real	ANFIS
3.264417	3.000
11.75883	10.140
15.14171	14.790
6.841045	6.380
14.57092	12.400
18.64209	18.100
29.04603	30.390
13.12156	13.000
15.42366	17.360
3.981349	4.210
5.914719	5.720
4.675447	4.940
3.299920	3.610
9.933099	8.400

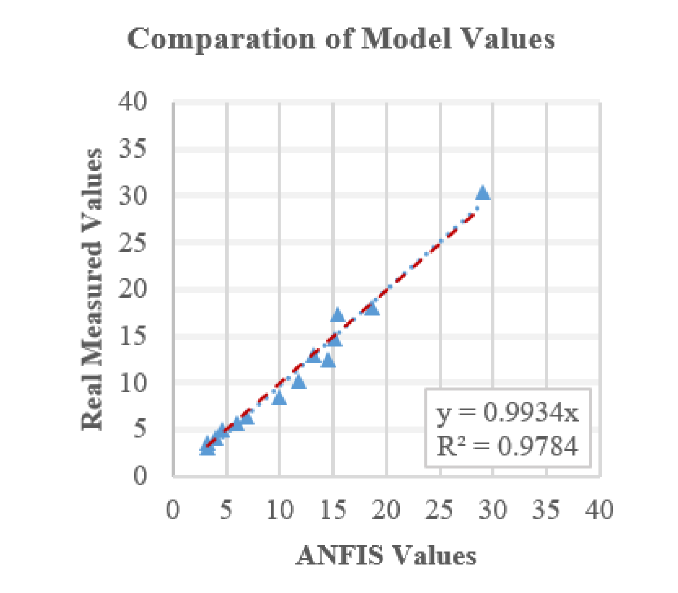

Comparison of Values of All Data

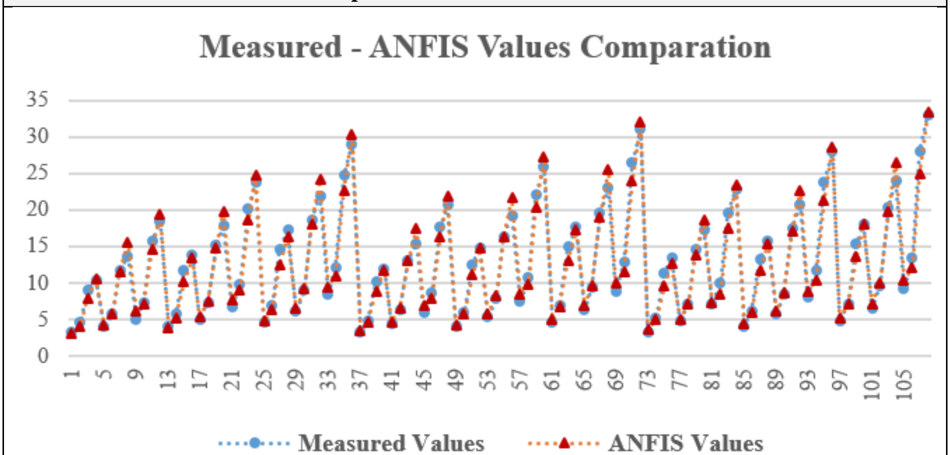

Table 2b: Statistical Scores (PM) by Selected Membership Functions

Inputs	X_1	X_2	X_3	X_4
MF	'dsigmf'	'gaussmf'	'gbellmf'	'trimf'
	Data Set	**Training**	**Test**	**Validation**
MAPE	0.1574	0.1333	0.1619	0.2492
MAE	0.3400	0.3005	0.3889	0.4489
RMSE	0.3795	0.3359	0.4186	0.4874
R^2	0.9536	0.9630	0.9453	0.9370

Training Dataset Measured and ANFIS-Generated Values

Real	ANFIS
2.0929788	1.720
3.3089761	2.790
2.5702163	2.120
1.0572701	1.470
4.8333818	5.330
3.7257418	4.070
2.293412	2.000
2.4655978	2.170
4.5885255	4.450
3.4358983	2.940
2.7074095	2.230
0.6833022	0.950
2.2756151	2.190
1.5550737	1.430
6.151119	6.650
1.494202	2.080
3.562693	3.030
6.800673	7.410

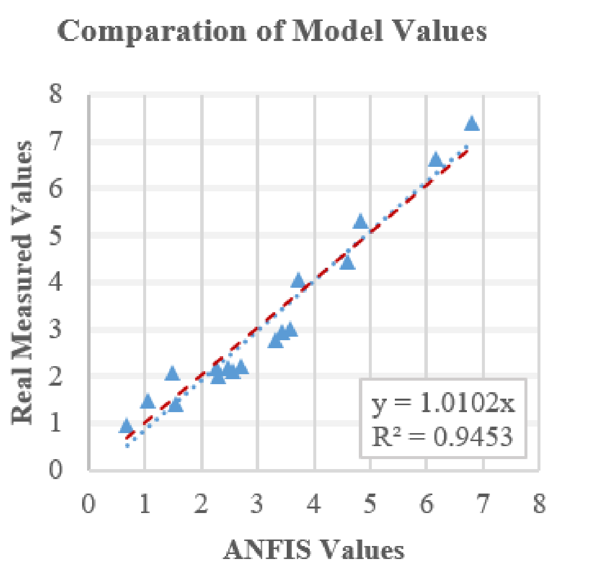

Comparison of Values of All Data

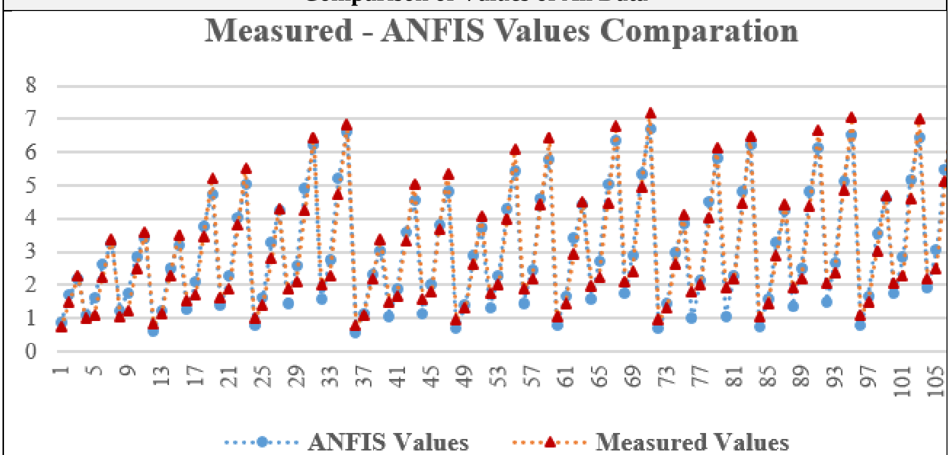

Table 2c: Statistical Scores (PAT) by Selected Membership Functions

Inputs	**X_1**	**X_2**	**X_3**	**X_4**
MF	'dsigmf'	'gaussmf'	'gbellmf'	'dsigmf'
	Data Set	**Training**	**Test**	**Validation**
MAPE	0.11395	0.11312	0.1224	0.1088
MAE	0.16425	0.15546	0.2075	0.1561
RMSE	0.20764	0.199127	0.2543	0.1881
R^2	0.96868	0.96960	0.9447	0.9777

Training Dataset Measured and ANFIS-Generated Values

Real	**ANFIS**
0.3368577	0.480
0.6276109	0.620
2.5425052	2.480
2.8795776	3.180
0.5882388	0.840
2.381754	2.200
3.1722474	2.980
2.0572626	2.470
2.6577771	2.520
3.2450863	3.190
2.3476824	1.920
1.1946176	1.190
1.7980226	1.440
3.2915908	2.960
2.9746244	3.440
2.475128	2.390
4.672416	4.950
0.618598	0.660

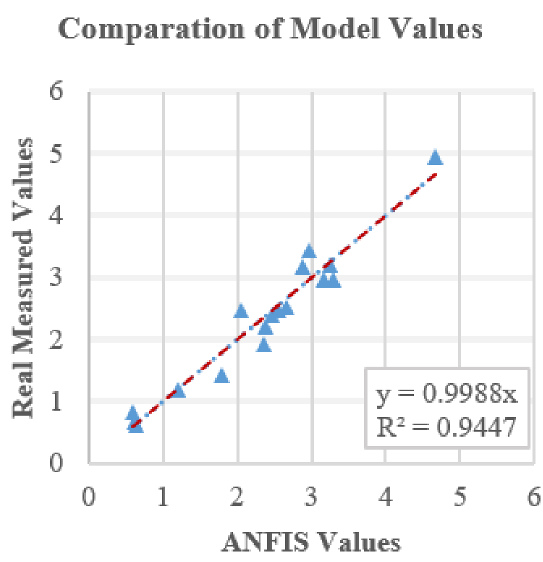

Comparison of Values of All Data

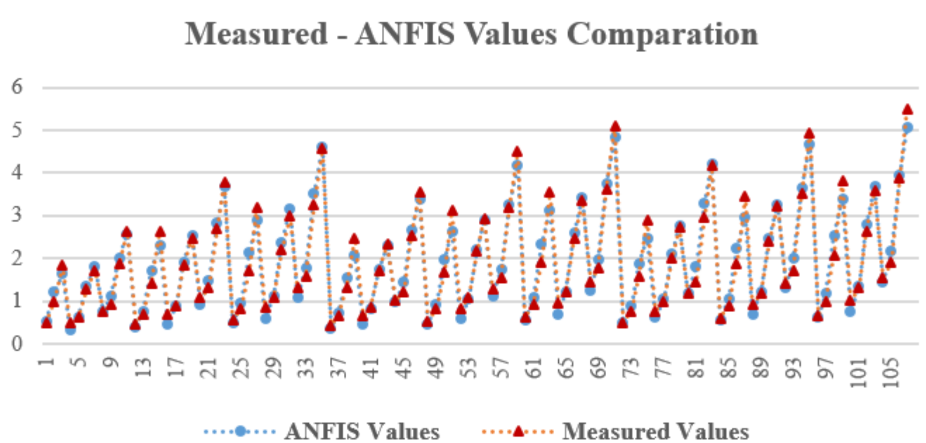

Table 2d: Statistical Scores (PMAT) by Selected Membership Functions

Inputs	X_1	X_2	X_3	X_4
MF	'dsigmf'	'gaussmf'	'gbellmf'	'dsigmf'
	Data Set	**Training**	**Test**	**Validation**
MAPE	0.09153	0.0917	0.10057	0.08146
MAE	0.90889	0.79827	1.3104	0.94982
RMSE	1.08700	0.95425	1.4470	1.16330
R^2	0.98770	0.98952	0.9785	0.98976

Training Dataset Measured and ANFIS-Generated Values

Real	ANFIS
7.0036975	7.960
8.0066045	6.690
15.485828	13.770
19.322181	17.840
7.3051136	6.850
11.544652	9.970
32.984008	34.850
9.2988878	10.480
6.937188	8.190
3.679104	3.590
11.162394	9.890
32.287274	34.550
9.3630212	8.380
14.927838	12.980
29.269954	29.750
9.726228	8.700
16.58213	14
30.49387	29.35

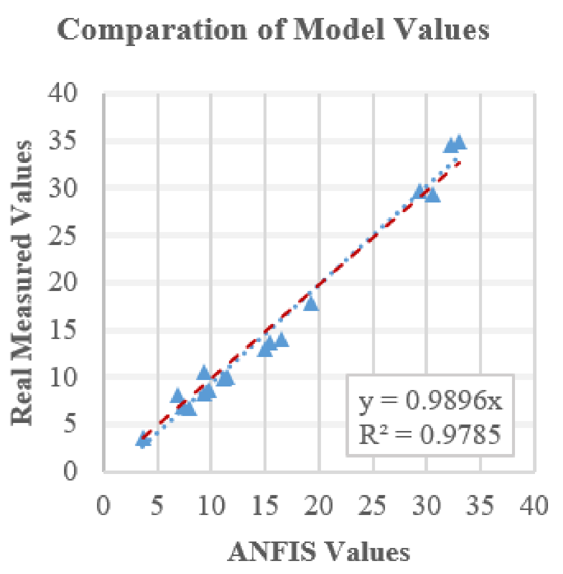

Comparison of Values of All Data

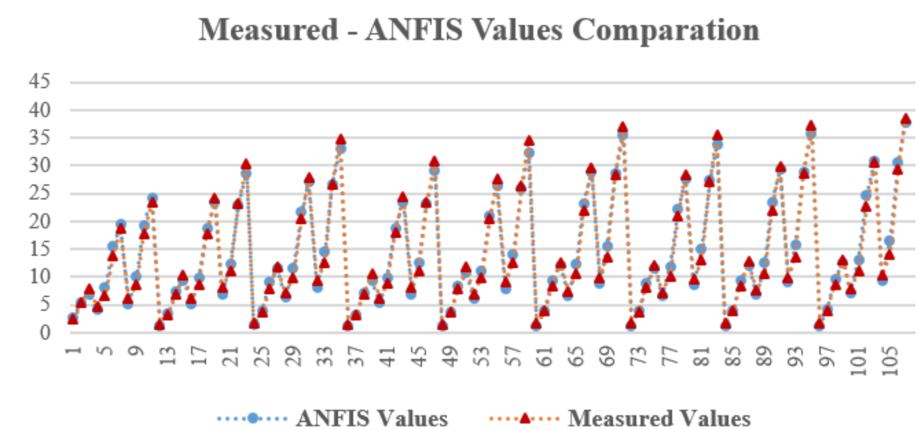

CONCLUSIONS

In this study, the wear properties of aluminium titanate and mullite doped porcelain ceramics. The obtained experimental wear test results were modelled with artificial neural networks. The results of the study are summarized below.

- As a result of wear tests, the amount of wear increased with increasing load and time.
- daptive Neuro Fuzzy Inference Systems, the training dataset was divided into 4 parts (Training, Testing, Validation and All data set).
- The highest R^2 values were calculated as 0.9785 in aluminium titanate and mullite doped porcelain.
- The MAPE, MAE and RMSE values obtained for the ANFIS model are 0.10057, 1.3104 and 1.4470 respectively for aluminium titanate and mullite doped porcelain.
- MAPE, MAE, RMSE and R^2 values of the obtained for All Data set are 0.09153, 0,90889, 1.08700 and 0.98770 for aluminium titanate and mullite doped porcelain.
- The smallest R^2 value was calculated in mullite added porcelain samples. While the R^2 value for the test set here is 0.9453, this value is calculated as 0.9536 for the all data set.

REFERENCES

Akkuş, A. and Boyraz T. (2019). Fabrication and characterization of aluminium titanate and mullite added porcelain ceramics. Journal of Ceramic Processing Research, 20(1),54-58.

Aksaf, I.A., Pask, J.A. (1983). Stable and Metastable Phase Equilibrium and reactions SiO2-Al2O3. Ceramics International, 9(4), 107-113.

Basheer, A. C. Dabade, U. A. Joshi, S. S. Bhanuprasad V.V. and Gadre, V.M. (2008). Modeling of surface roughness in precision machining of metal matrix composites using ANN, Journal of Materials Processing Technology, Journal of Materials Processing Technology, 97(1-3),439-444.

Baudín, C., Tricoteaux, A.A., Joire, H. (2014). Improved resistance of alumina to mild wear by aluminium titanate additions. Journal of the European Ceramic Society, 34, 69-80.

Buckley, D.H., Miyoshi, K. (1984). Friction and wear of ceramics. Wear, 100(1-3),333-353.

Boyraz, T. and Akkuş, A. (2021). Investigation of wear properties of mullite and aluminium titanate added porcelain ceramics. Journal of Ceramic Processing Research, 22(2),226-231.

Chargui, F., Hamidouche, M., Belhouchet, H., Jorand, Y., Doufnoune, R., Fantozzi, G. (2018). Mullite fabrication from natural kaolin and aluminium slag. Boletin de la Sociedad Española de Cerámica y Vidrio, 57,169-177.

Chollet, F. (2018). Deep Learning with Python. Manning Public. NY. USA.

Çıtak, E., Boyraz, T. (2014). Microstructural characterization and thermal properties of aluminium titanate/YSZ ceramics. Acta Physica Polonica A, 125(2),465-468.

Hassan, A., Alrashdan, M. A., Hayajneh, M.T., Mayyas, A. T. (2009). Prediction of density, porosity and hardness in aluminum–copper-based composite materials using ANN. Journal of Materials Processing Technology, 209, 894-899.

Hillig, W. (1993). A Methodology for Predicting the Mechanical Properties of Oxides at High Temperatures. Journal of the American Ceramic Society, 76(1), 129-138.

Huang, C., Zhang, Z. L., He, L., Sun, J., Fang, B., Zou, B., Li Z. Q. and Ai, X. (2002). A study on the prediction of the mechanical properties of a ceramic tool based on an artificial neural network, Journal of Materials Processing Technology, 129(1-3),399-402.

Jang, J.S.R. (1993). ANFIS: Adaptive-Network-Based Fuzzy Inference System. IEEE Transactions on Systems Man and Cybernetics, 23(3), 665-685.

Jiang, L., Chen, X. Y., Han, G. M. and Yu, M. E. N. G. (2011). Effect of additives on properties of aluminium titanate ceramics. Transactions of Nonferrous Metals Society of China, 21: 1574-1579.

Jiang, Z, Zhang, Z. and Friedrich, K. (2007). Prediction on wear properties of polymer composites with artificial neural networks. Composites Science and Technology, 67(2),168-176.

Karaboga, D., & Kaya, E. (2022). Adaptive Neuro-Fuzzy Inference System (ANFIS) Training Based on Artificial Bee Colony (ABC) Algorithm. Applied Soft Computing, 105, 107275.

Karaboga D. and Kaya, E. (2019). Adaptive network based fuzzy inference system (ANFIS) training approaches: a comprehensive survey. Artificial Intelligence Review, 52(4), 2263-2293.

Koker, R., Altinkok, N. and Demir, A. (2007). Neural network based prediction of mechanical properties of particulate reinforced metal matrix composites using various training algorithms. Materials & Design, 28, 616-627.

Kong Y, Yang Z, Zhang G, Yuan Q. (1998). Friction and wear characteristics of mullite, ZTM and TZP ceramics. Wear, 218,159-66.

Kucuk, I., Boyraz, T., Gokce, H., Ovecoglu, M.L. (2018). Thermomechanical properties of aluminium Titanate (Al_2TiO_5)-reinforced forsterite (Mg_2SiO_4) ceramic composites. Ceramic International, 44(7),8277-8282.

Lee, E.J., Iqbal Y. (2001). Influence of mixing on mullite formation in porcelain. Journal of the European Ceramic Society, 21, 2583-2686.

Lin, C.T., & Lee, C.S.G. (1996). Neural Fuzzy Systems: A Neuro-Fuzzy Synergism to Intelligent Systems. Prentice-Hall International.

Mandal, S., Sivaprasad, P.V., Venugopal, S., Murthy, K.P.N. (2009). Artificial neural network modelling to evaluate and predict the deformation behaviour of stainless steel type AISI 304L during hot torsion. Applied Soft Computing, 9, 237-244.

Marquez, J.M., Rincon, J.M., Romero, M. (2008). Effect of firing temperature on sintering of porcelain stoneware tiles. Ceramic International, 34,1867-1873.

Marquez, J.M., De la Torre, A.G., Aranda, M.A.G., Rincon, J.M., Romero, M. (2009). Evolution with temperature of crystalline and amorphous phases in porcelain stoneware. Journal of the American Ceramic Society, 92, 229-234.

Mendel, J.M., & John, R.I. (2020). Type-2 Fuzzy Logic: Theory and Applications. IEEE Transactions on Fuzzy Systems, 28(10), 2130-2148.

Ozsoy, E., Onen, U., Boyraz, T. (2015). Microstructural characterization and thermal properties of aluminium titanate/talc ceramic matrix composites.

Acta Physica Polonica A, 127(4),1136-1138.

Önen, U., Boyraz, T. (2014). Microstructural characterization and thermal properties of aluminium titanate/spinel ceramic matrix composites. Acta Physica Polonica A, 125(2),488-491.

Russell, S., & Norvig, P. (2020). Artificial Intelligence: A Modern Approach. Pearson

Saclı, M., Onen, U., Boyraz, T. (2015). Microstructural characterization and thermal properties of aluminium titanate/porcelain ceramic matrix composites. Acta Physica Polonica A, 127(4),1133-1135.

Serra, M.F., Conconi, M.S., Gauna, M.R., Suárez, G., Aglietti, E.F., Rendtorff, N.M. (2016). Mullite ($3Al_2O_3 \cdot 2SiO_2$) ceramics obtained by reaction sintering of rice husk ash and alumina, phase evolution, sintering and microstructure. Journal of the Asian Ceramic Society, 4, 61-67.

Sopeña, J.M.G., Pakrashi, V., Ghosh, B. (2021). An overview of performance evaluation metrics for short-term statistical wind power forecasting, Renewable and Sustainable Energy Reviews, 138, 110515.

Talpur, N. M., Salleh, N. M., Hussain, K. (2017). An investigation of membership functions on performance of ANFIS for solving classification problems, IOP Conf. Ser.: Materials Science Engineering, 226, 012103.

Takagi, T., & Sugeno, M. (1985). Fuzzy identification of systems and its applications to modeling and control. IEEE Transactions on Systems, Man, and Cybernetics, 15(1), 116-132.

Tsoukalas L. H. and Uhrig, R. E. (1996). Fuzzy and Neural Approaches in Engineering, 1st ed. New York, NY, USA. John Wiley & Sons, Inc.

Ye, L., Lu, Y., Su, Z., Meng, G. (2005). Functionalized composite structures for new generation airframes: a review. Composites Science and Technology, 65, 1436-1446.

Yu, L. Wang, S., Lai, K. K. (2006). An integrated data preparation scheme for neural network data analysis, IEEE Transactions on Knowledge and Data Engineering, 18(2), 217-230

Yüksek, A. G., Elagöz, S., Şenadım, E.T. (2015). Modeling of reflectance properties of ZnO film using artificial neural networks. Journal of Optoelectronics and Advanced Materials, 17, 1675-1628.

Yüksek, A.G. (2007). Comparison of Multiple Regression Analysis and Artificial Neural Networks Method in Air Pollution Prediction. PhD Thesis, Cumhuriyet University, Sivas, Turkey.

Zadeh, L. A. (1965). Fuzzy sets. Information and Control, 8(3),338-353.

Zadeh, L.A. (2021). From Computing with Numbers to Computing with Words. From Manipulation of Measurements to Manipulation of Perceptions. IEEE Transactions on Circuits and Systems I: Regular Papers, 68(1), 1-18.

Chapter 3

Mathematical Thermal Stress Analysis in Metal-Ceramic and Ceramic-Ceramic Coatings

Tahsin BOYRAZ[1]

[1] Sivas Cumhuriyet University, Metallurgical and Materials Engineering, Sivas, Turkey
tahsinboyraz@cumhuriyet.edu.tr ORCID No: 0000-0003-4404-6388

Abstract

The fact that experimental studies are expensive and take a lot of time has made shorter and less costly modelling methods important. The purpose of this study was to investigate the effect of heat changes in oral environment producing thermal stresses in dental restorations by a mathematical method and to compare with bond strength values obtained from experimental studies. Thermal stress was calculated mathematically for seven different ceramic-on-ceramic and six different ceramic-on-metal systems. Mathematically, thermal stress calculations were made according to the Boley equation. Elastic modulus (E), Poisson ratio (ν), coefficient of thermal expansion (α) and bond strength values of the materials used in mathematical modelling were taken from manufacturers' websites and literature reports. The average experimental bond strength in the ceramic-ceramic structure is 32.03±6.70 MPa and this value was calculated as 2.16±1.85 MPa in mathematical analysis. Similarly, the average value between ceramic- metal while it is 48.90±9.87 MPa, it was mathematically calculated as 4.05±2.54 MPa. As a result, there is a temperature-related stress in dental restorations, but it has been calculated that this is not to the extent of damaging the restoration.

Keywords: Thermal stress, Mathematical Modelling, Ceramics, Metal, Bond strength.

INTRODUCTION

Dental materials are a part of systems designed to produce dental prostheses that are used due to aesthetic concerns or to replace missing or damaged tooth structures. There are many metal, ceramic, glass-ceramic, polymer, composites such as materials used in dental restorations. Many materials such as composite resin and calcium-silicate cements, yttria-stabilized zirconia, geopolymer-derived leucite, lithium disilicate, spinell, alumina, feldispatic ceramic, hydroxyapatite, CrNiMo, CrCoMo, Ti, Ti6Al4V, gold and palladium alloys etc. are used in dental restorations (Rezaie,2020; Dimitrova,2023).

Many properties of the materials such as physical, chemical, mechanical, thermal and biological are important for long-term use of artificial teeth in the oral environment. Some of these properties are colour, density, thermal stress, strength, hardness, polymerization, biocompatibility (Yadav and Kumar, 2019; Warreth and Elkareimi, 2020). Elastic modulus and Poisson's ratio are among the mechanical properties and parameters that measure the elastic or plastic strain behaviour of dental materials. On the other hand, thermal expansion coefficient is also one of the thermal properties of materials. Elastic modulus (E, MPa), Poisson ratio (ν), Temperature (T) and Coefficient of Thermal Expansion (CTE, α, x10^{-6}. K^{-1}.) are very important parameters in thermal stress studies and calculations (Boley and Weiner, 2013).

Artificial dental materials are exposed to many factors that affect their use in vivo. Heat transfer and thermal shocks in teeth occur both in daily life and in dental surgery. The thermal environment of teeth in daily life varies over a wide temperature range. The highest temperature during hot beverage consumption was measured between the lower incisors and the maximum value was reached at 76.3oC. Thermal changes during feeding in the oral cavity vary between -5 and 76.3 oC. Under these conditions, differences in thermal and physical properties between dental restorative materials facilitate the development of thermal stress, especially in the oral cavity. This difference, together with the stresses resulting from chewing and temperature change, affects the bond strength, especially at the metal-ceramic and ceramic-ceramic interface (Haskan et.al., 2007; Coskun et.al., 2015; Vojdani et.al., 2012).

Nowadays, prediction and classification studies with artificial intelligence are increasing rapidly. Prediction with machine learning requires a large number of experimental data in the same group. Therefore, a mathematical modelling was used in this study. Real experimental data was used here too but it is incomparably less than modelling with artificial intelligence.

The aim of this study is to mathematically calculate the thermal stresses that will occur at the interfaces in metal-ceramic and ceramic-ceramic restorations in different temperature environments, without taking into account mechanical and physical effects, only due to the temperature difference. Afterwards, the bond strength values obtained from the literature will be compared with the values obtained by mathematical analysis.

MATERIALS AND METHODS

In dental restorations, metal-on-ceramic and ceramic-on-ceramic artificial tooth applications prepared externally through various stages are then placed in the mouth appropriately. In this study, mathematical calculation and modelling of the thermal expansions caused by the temperature difference during eating of artificial teeth produced for this purpose and mounted in the mouth will be made. Elastic modulus (E, MPa), Poisson ratio (ν) and coefficient of thermal expansion (CTE, α, x10-6. K-1.) values of the materials used in mathematical modelling were taken from manufacturers' websites and literature. Some values that are not available have also been calculated theoretically (Table 1 and 2) (Haskan, 2007; Coskun, 2015; Vojdani, 2012; Lunt, 2015; Bona, 2008; Ertürk, 2015; Hsueh, 2008; Longhini, 2016; Wood, 2008; Wiedenmann, 2021; Trindade, 2018; Wang, 2019; Yoshimura, 2012; Ganesh, 2013; Tribst, 2021; Archangelo, 2019; Dai, 2018; Ma, 2013; Borba, 2011; Borba, 2015; Guazzato, 2002; Khmaj, 2014; Albakry, 2003; Chantranikul, 2015; Suansuwan, 2001; Benetti, 2010; DeHoff, 1998; Abtahi, 2022; Madeira, 2019; Rynıewıcz, 2020; Zhang, 2013).

The thermal stress (σ, MPa) calculations were made according to the Boley equations. In the Boley equation, the elastic modulus of the material 'E', thermal expansion coefficient 'α', temperature change 'T' and Poisson's ratio 'ν' are the effective parameters (Boley and Weiner, 2013). For the mathematical investigation of thermal stresses, in Fig. 1 the stress-strain state of a free tooth structure is shown in the form of a plate. In calculating these stresses that will affect the bond strength, a total thickness of 1 mm was chosen, including 0.5 mm substructure and 0.5 mm veneering material. n the calculations, the temperature was taken as minimum -5 and maximum 76.3 ^{o}C (Haskan, 2007; Coskun, 2015; Vojdani, 2012; Lin, 2010; Jacobs, 1973; Feuerstein, 2008).

The entire thickness of the restoration was assumed to be 1 mm and this thickness is expressed as 2h in the formula. The structure of the material is completely independent of the surface traction and the stresses depend only on the thickness, the temperature varies through the thickness only, that is, T= T(z). Under these conditions, the thermal stress components that occur in the middle of the structure due to the temperature change along the physical thickness will be calculated by the formulas given below.

Table 1: Manufacturers and chemical compositions of ceramic and metal materials used in calculations

Brand name	Chemical compositions, %
Vita VM7	SiO_2 (66-70), Al_2O_3(13-17), K_2O (9-10), Na_2O (3-4), CaO (2-3), ZrO_2(0-1), Y_2O_3(0,07-0,23)
Vita VM9	SiO_2 (60-64), Al_2O_3(13-15), K_2O (7-11), Na_2O (4-6), B_2O_3(3-5), BaO (1-3), CaO (1-2), ZrO_2 (0-1)
Vita VM13	SiO_2 (59-63), Al_2O_3(13-16), K_2O (9-11), Na_2O (4-6)
Vita VM15	SiO_2 (41,3), Al_2O_3(14,5), K_2O (14), Na_2O (3), SnO_2(11,9), ZrO_2(5,8), CaO (4,4), P_2O_5(4,1)
Vita Titankeramik	SiO_2 (60-62), Al_2O_3(7-8), K_2O (7-7,6), Na_2O (5-5,7), CaO (1,0-1,3), B_2O_3(6-7), BaO (0,1-0,3), SnO_2(2,1-2,7), MgO (6,0-4,4), TiO_2(5,0-5,4)
Vita In-Ceram Alumina	75% Al_2O_3, 25% infiltration glass
Vita In-Ceram Spinel	78% $MgAl_2O_4$, 22% infiltration glass
Vita In-Ceram Zirconia	56% Al_2O_3, 24% Ce-ZrO_2, 20% infiltration glass
Vita In-Ceram AL	100% Al2O3
Vita In-Ceram YZ	92%ZrO_2, 5%Y2O3, HfO_2< 3%, Al_2O_3 and SiO_2< 1%
Vita Vitablocs	SiO_2 (56-64), Al_2O_3(20-23), Na_2O(6-9), K_2O(6-8), other
Vita PM 9	SiO_2 (62-67), Al_2O_3 (16-19), K_2O (6-8), Na_2O (5-8), B_2O_3 (1-3)
Bego, Bio PontoStar XL, Au	Au86.0Pt11.5Zn1.6FeInRh
Bego, BegoPal 300, Pd	Pd75.4In6.3Ag6.2Au6.0Ga6.0Ru
Bego, Wirobond SG, CrCo	Co63.8Cr24.8W5.3Mo5.1Si1.0 [%])
Bego, Wiron 99, NiCr	Ni 65.0, Cr 22.5, Mo 9.5, Nb 1.0, Si 1.0, Fe0.5, Ce 0.5, C max. 0.02
Dentaurum Rematitan Ti2	Ti%99,3, other < 1%
Dentaurum Rematitan Ti5	Ti6Al4V- 89% Ti, 6% Al, 4% V, other 1%

In calculating these stresses that will affect the bond strength, a total thickness of 1 mm was chosen, including 0.5 mm substrate and 0.5 mm coating material. In calculating these stresses that will affect the bond strength, a total thickness of 1 mm was chosen, including 0.5 mm substructure and 0.5 mm veneering material. n the calculations, the temperature was taken as minimum -5 and maximum 76.3 ^{o}C.

This special study on thermal stresses were built on thermal stresses resulting from temperature changes in the physical and mechanical characteristic thickness of metal-ceramic and ceramic-ceramic restorations.

$$\sigma_{xx} = \sigma_{yy} = f(z), \sigma_{zz} = \sigma_{xz} = \sigma_{yx} = \sigma_{zy} = 0 \quad (1)$$

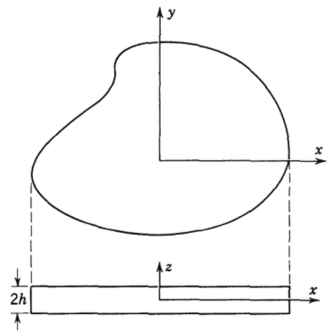

Figure 1. The scheme of the plate

The balance conditions are indistinguishably fulfilled for push components of this frame. For strain components criteria for fulfilling the balance may be communicated as takes after:

$$\frac{d^2}{dz^2}\left[f + \frac{\alpha E}{1-\nu} T \right] = 0 \tag{2}$$

where α is thermal expansion coefficient of the plate material. The solution of the eq. 2 can be given as follows:

$$\sigma_{xx} = \sigma_{yy} = f = C_1 + C_2 z - \frac{E\alpha T}{1-\nu} \tag{3}$$

Where are defined as the elastic modulus 'E', the coefficient of thermal expansion 'α', the temperature change 'T' and the Poisson ratio 'ν' of the plate material. The form of nonzero stress components can be given by solving eq.2 as follows. Integral constants, C_1 and C_2 in eq.3 can only be present provided that the stresses are zero on the edges of the plate (Boley and Weiner, 2013).

where the constants C_1 and C_2 are to be determined from the boundary conditions of zero tractions on the edges of the plate. For any temperature T(z) it is possible to choose constants C_1 and C_2 such that the resultant force and moment (per unit of length) produced by σ_{xx} and σ_{yy} are zero on the edges of the plate.

$$\int_{-h}^{h} \sigma_{xx} dz = \int_{-h}^{h} \sigma_{xx} z dz = \int_{-h}^{h} \sigma_{yy} dz = \int_{-h}^{h} \sigma_{yy} z dz = 0 \tag{4}$$

The solution is then found to be:

$$\sigma_{xx} = \sigma_{yy} = \frac{\alpha E}{1-\nu}\left\{ -T + \frac{1}{2h}\int_{-h}^{h} T dz + \frac{3z}{2h^3}\int_{-h}^{h} T z dz \right\} \tag{5}$$

According to Saint-Venant's principle this solution is a quite accurate approximation for traction-free edges at distance from these edges larger than about one plate thickness. Since the requirement that the plate faces z=±h is free of traction is clearly satisfied by eq.1, the above solution is, within the approximation corresponding to Saint-Venant’s principle, the desired (end unique) solution of the stated thermos elastic boundary-value problem (Boley and Weiner, 2013).

The constants C_1 and C_2 can be calculated with the 6th and 7th equations given below. Calculations are made by substituting these constants in equation 3.

$$C_1 \int_{-h}^{h} \frac{E}{1-v} dz + C_2 \int_{-h}^{h} \frac{E}{1-v} z dz - \int_{-h}^{h} \frac{T\alpha E}{1-v} dz = 0 \qquad (6)$$

$$C_1 \int_{-h}^{h} \frac{E}{1-v} z dz + C_2 \int_{-h}^{h} \frac{E}{1-v} z^2 dz - \int_{-h}^{h} \frac{T\alpha E}{1-v} z dz = 0 \qquad (7)$$

Table 2. Elastic modulus (E, GPa), Poisson ratio (ν) and coefficient of thermal expansion (α, CTE, x10^{-6}. K^{-1}) of ceramic and metal materials used in thermal stress studies and calculations.

Materials		**E**	**CTE**	**ν**
Ceramic-Ceramic				
VM7	Veneering	66 ± 6,2	7,1 ± 0,1	0,21 ± 0,02
In-Ceram Alumina	Substructure	270 ± 10,0	7,4 ± 0,2	0,25 ± 0,02
In-Ceram Spinel	Substructure	282 ± 3,0	7,7 ± 0,2	0,27 ± 0,02
In-Ceram Zirconia	Substructure	240 ± 10,0	7,7 ± 0,1	0,26 ± 0,02
In-Ceram AL	Substructure	375 ± 25,0	7,7 ± 0,3	0,22 ± 0,01
VM9	Veneering	66 ± 1,2	9,1 ± 0,1	0,21 ± 0,01
In-Ceram YZ	Substructure	207 ± 4,0	10,5 ± 0,5	0,30 ± 0,01
Blocs	Substructure	45 ± 2,0	9,4 ± 0,1	0,30 ± 0,01
PM9	Substructure	64 ± 2,5	9,3 ± 0,2	0,21 ± 0,02
Ceramic-Metal				
VM13	Veneering	69 ± 2,0	13,4 ± 0,2	0,21 ± 0,01
Bio PontoStar XL, Au,	Substructure	100 ± 10,0	14,3 ± 0,2	0,41 ± 0,02
BegoPal 300, Pd	Substructure	135 ± 5,0	13,9 ± 0,2	0,40 ± 0,01
VM15	Veneering	71 ± 2,0	15,6 ± 0,1	0,20 ± 0,01
Wirobond SG, CrCo	Substructure	200 ± 10,0	14,4 ± 0,2	0,29 ± 0,01
Wiron 99, NiCr	Substructure	170 ± 20,0	13,9 ± 0,1	0,29 ± 0,01
Titankeramik	Veneering	91 ± 2,0	8,6 ± 0,3	0,20 ± 0,01
Rematitan Ti2, Ti	Substructure	120 ± 10,0	9,6 ± 0,2	0,36 ± 0,01
Rematitan T5,Ti6Al4V	Substructure	120 ± 10,0	10,0 ± 0,2	0,34 ± 0,01

By utilizing the conditions gotten, warm stresses shaped at the association of metal-ceramic and ceramic-ceramic, which is broadly utilized in dental medicines, were explored on the condition that the temperature variety is homogeneous. For this application values from Table 2 were utilized.

RESULTS AND DISCUSSION

Temperature-dependent thermal stresses were calculated mathematically with the help of the Boley equation (Table 3 and Fig.2). According to the results obtained, thermal stresses increase with increasing temperature.

Table 3. Thermal stresses (MPa) calculated by mathematical method at the ceramic-ceramic and ceramic-metal interface.

Veneering material	Substructure material	-5 °C	37,5 °C	76,3 °C
Vita VM7	Vita In-Ceram Alumina	0,211	1,580	3,214
Vita VM7	Vita In-Ceram Spinel	0,444	3,329	6,774
Vita VM7	Vita In-Ceram Zirconia	0,389	2,920	5,940
Vita VM7	Vita In-Ceram Al	0,519	3,894	7,923
Vita VM9	Vita In-Ceram YZ	0,536	4,017	8,172
Vita VM9	VitaBlocs	0,061	0,454	0,925
Vita VM9	Vita PM9	0,042	0,312	0,635
Vita VM13	Bego, Bio PontoStar XL, Au,	0,348	2,612	5,315
Vita VM13	Bego, BegoPal 300, Pd	0,245	1,837	3,738
Vita VM15	Bego, Wirobond SG, CrCo	0,707	5,302	10,788
Vita VM15	Bego, Wiron 99, NiCr	0,879	6,591	13,411
Vita Titankeramik	Dentaurum, Rematitan Ti2, Ti	0,201	1,511	3,074
Vita Titankeramik	Dentaurum, Rematitan T5,Ti6Al4V	0,279	2,094	4,261

As a result of the calculations, it was observed that the stresses occurring at the ceramic-metal interface were generally higher. In ceramic-ceramic restorations, the highest value was calculated as 8.172 MPa at the VitaVM9 and Vita In-Ceram YZ interface and at 76.3 °C. However, this value was calculated as 13.411 at 76.3 °C for Vita VM15 - NiCr alloy (Bego, Wiron 99) at the ceramic-metal interface.

These differences arise from the effective parameters in the calculations: elastic modulus (E), the coefficient of thermal expansion (α), the Poisson ratio (ν) of the materials.

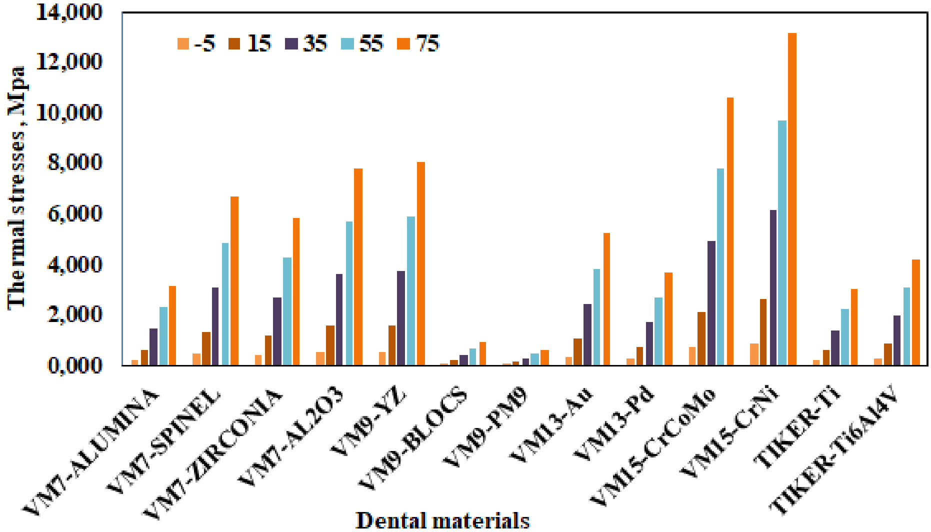

Figure 2: Some mathematically calculated thermal stress results.

Table 4. Average bond strength (MPa) values of some ceramic - ceramic and metal - ceramic systems used in dental restorations.

Veneering material	Substructure material	bond strength
Ceramic	In-Ceram Alumina	25,60 ± 10,90
Ceramic	In-Ceram Spinel	37,35 ± 10,75
Ceramic	In-Ceram Zirconia	24,60 ± 9,6
Ceramic	In-Ceram Al2O3	38,80 ± 6,3
Ceramic	In-Ceram YZ	33,81 ± 7,96
Ceramic	Au Alloys	49,50 ± 14,80
Ceramic	Pd Alloys	52,46 ± 15,26
Ceramic	CrCoMo Alloys	39,50 ± 6,50
Ceramic	NiCrMo Alloys	37,53 ± 14,99
Ceramic	Titanium (Ti)	42,00 ± 18,00
Ceramic	Ti6Al4V	72,39 ± 20,12

Benetti, Kern, Kim, Valandro et al. tested the ceramic-alumina bond strengths in the ceramic-ceramic system in different studies they conducted. The average bond strength value of these studies was calculated as 25.60 ± 10.90 MPa. In a study investigating a new retention system for In-Ceram and In-Ceram Spinell ceramics, Wood et al. found the ceramic-in-ceram spinell bond strength to be 37,35 ± 10,75 MPa on average. They investigated the effect of surface conditioning on the bond strength of resin cement to high alumina and zirconia reinforced ceramics and found the bond strength to be 26,8+-7,4 MPa. When similar studies are evaluated, the average bond strength of ceramic-in ceram zirconia restorations is 24.60+-9.60 MPa (Benetti, 2010; Kern, 1995; Kim, 2005; Valandro, 2006; Wood, 1997).

In an in vitro study evaluating the tensile bond strength and adhesive bonding systems of dense sintered alumina ceramic, Hummel et al. found the bond strength to be 38,80 ± 6,3 MPa. The average bond strength obtained from studies investigating the effects of thermal expansion coefficient, thermal incompatibility and surface conditioning on the bond strength of ceramic-coated yttrium-stabilized zirconia is 33,81 ± 7,96 MPa (Valandro, 2006; Wood, 1997; Hummel, 2004; Juntavee, 2018; Komine, 2012; Fischer, 2009; Saito, 2010).

Khmaj et al. investigated of the comparison of metal-ceramic bonding strengths of gold alloys with metal pressing and traditional porcelain layering techniques. Vásquez et al. studied the interface characterization and evaluation of the adhesion of glass ceramics to gold alloy after thermal and mechanical loading. As a result of the evaluation of these studies with similar studies, the average ceramic-gold bond strength was found to be 49,50 ± 14,80 MPa [44,62,63]. Lopes et al. studied the correlatıon Between palladium-ceramıc bond strength and coeffıcıent of lınear thermal expansıon. Khmaj et al. investigated of the comparison of metal-ceramic bonding strengths of palladium alloys with metal pressing and traditional porcelain layering techniques. As a result of the evaluation of these studies with similar studies, the average ceramic-palladium bond strength was found to be 52,46 ± 15,26 MPa (Khmaj, 2014; Saito, 2010; Vásquez, 2009; Lopes, 2009).

In the bond strength studies of Ni-Cr based alloys with ceramics reached values; Neto et al. 22.54-35.11 MPa, Lopes et al. 38.61-43.12 MPa and Czepułkowska et al. 40.48-52.52 MPa. The average ceramic-NiCr alloys bond strength was found to be 37,53 ± 14,99 MPa. In porcelain studies on CoCr alloys; Neto et al. investigated the bond strength of three dental porcelains to CoCr Alloys. Czepułkowska et al. studied the role of mechanical, chemical and physical bonds in CoCr-ceramic bond strength. Kaleli and Saraç comparised of porcelain bond strength of different metal frameworks. The average ceramic-CoCr alloys bond strength was found to be 39,50 ± 6,50 MPa (Lopes, 2009; Neto, 2006; Czepułkowska, 2018; Kaleli, 2017).

In some studies, on Ti-dental porcelain bond strength, an average value of 42,00 ± 18,00 MPa was reached [53,68-71]. Toptan et al. investigated the influence of the processing route of porcelain/Ti–6Al–4V interfaces on shear bond strength. Sendão et al. studied the the effect of thermal cycling on the shear bond strength of porcelain/Ti–6Al–4V interfaces. The average bond strength value obtained as a result of these studies is 72,39 ± 20,12 MPa (Zhang, 2013;

Atsü, 2000; Lubas, 2020; Zinelis, 2010; Bondioli, 2004; Toptan, 2013; Sendão, 2015).

Table 5. General average bond strength (MPa) and calculated average thermal stress (MPa) values in ceramic - ceramic and metal - ceramic systems used in dental restorations.

Veneering material	Substructure material	Bond Strength	Thermal Stress
Ceramic	Ceramic	32,03 ± 6,70	2,16±1,85
Ceramic	Metal	48,90 ± 9,87	4,05±2,54

The main purpose of this study is to calculate the thermal stresses that will occur with temperature changes in the ceramic-ceramic and ceramic-metal connection area in dental restorations with a mathematical method and to compare and the obtained values with the experimental bond strengths. In Table 4, average bond strength values of some ceramic - ceramic and metal - ceramic systems used in dental restorations are given separately. The general average bond strength and calculated average thermal stress values of ceramic-ceramic and metal-ceramic systems used in dental restorations are given in Table 5.

While the general average experimental bond strength in the ceramic-ceramic structure is 32.03 ± 6.70 MPa, this value was calculated as 2.16 ± 1.85 MPa in mathematical calculation. Similarly, the general average value between ceramic-metal While it is 48.90 ± 9.87 MPa, it was mathematically calculated as 4.05 ± 2.54 MPa. There is a temperature-related stress in dental restorations, but it has been observed that this is not to the extent of damaging the restoration.

CONCLUSION

Based on the findings of this mathematical analysis study, the following conclusions were drawn:

- Elastic modulus, thermal expansion coefficient and Poisson ratio properties of ceramic and metal materials were effective in temperature-dependent thermal stresses.
- Thermal stress and bond strength values, both mathematically calculated and obtained from experimental data, were higher in ceramic-metal restorations.
- Experimentally obtained bond strength values are much higher than mathematically calculated thermal stresses.
- According to the results obtained from mathematical analysis and experimental bond strength comparison, it has been shown that the effect of thermal stresses alone cannot break the ceramic-ceramic and metal-ceramic bond strength.

REFERENCES

Abtahi, S., Alikhasi, M., Siadat, H. (2022). Biomechanical behavior of endocrown restorations with different cavity design and CAD-CAM materials under a static and vertical load: A finite element analysis. Journal of Prosthetic Dentistry,127(4), 600.e1-600.e8.

Albakry, M., Guazzato, M., Swain, M.V. (2003). Biaxial flexural strength, elastic moduli, and x-ray diffraction characterization of three pressable all-ceramic materials. Journal of Prosthetic Dentistry, 89(4),374-380.

Archangelo, K.C., Guilardi, L.F., Campanelli, D., Valandro, L.F., Borges, A.L.S. (2019). Fatigue failure load and finite element analysis of multilayer ceramic restorations. Dental Materials, 35(1),64-73.

Atsü, S., Berksun, S. (2000). Bond strength of three porcelains to two forms of titanium using two firing atmospheres. Journal of Prosthetic Dentistry, 84(5),567-574.

Benetti, P., Della Bona, A., Kelly, J.R. (2010). Evaluation of thermal compatibility between core and veneer dental ceramics using shear bond strength test and contact angle measurement. Dental Materials, 26(8),743-50.

Boley, B.A., Weiner, J.H. (2013). Theory of Thermal Stresses. New ed.(corrected). New York, Mineola.

Bona, A. D., Mecholsky, J.J. Barrett, A.A. Griggs, J.A. (2008). Characterization of glass-infiltrated alumina-based ceramics. Dental Materials, 24(11),1568-74.

Bondioli, I.R., Bottino, M.A. (2004). Evaluation of shear bond strength at the interface of two porcelains and pure titanium injected into the casting mold at three different temperatures. Journal of Prosthetic Dentistry, 91(6),541-547.

Borba, M., de Araújo, M.D., de Lima, E., Yoshimura, H.N., Cesar, P.F., Griggs, J.A., Della Bona, A. (2011). Flexural strength and failure modes of layered ceramic structures. Dental Materials, 27(12),1259-1266.

Borba, M., Duan, Y., Griggs, J.A., Cesar, P.F., Della Bona, Á. (2015). Effect of ceramic infrastructure on the failure behavior and stress distribution of fixed partial dentures. Dental Materials, 31(4),413-22.

Coskun, M.E., Boyraz, T., Tugut, F., Akin, H. (2015). Investigation of Thermal Stress in Different Metal Based Dental Restorations by Mathematical Analysis. Cumhuriyet Dental Journal,18(4),311-317.

Czepułkowska, W., Wołowiec-Korecka, E., Klimek, L. (2018). The role of mechanical, chemical and physical bonds in metal-ceramic bond strength. Archives of Materials Science and Engineering, 92(1),5-14.

Chantranikul, N., Salimee, P. (2015). Biaxial flexural strength of bilayered zirconia using various veneering ceramics. Journal of Advanced Prosthodontics, 7(5),358-67.

Dai, K., Shaw, L. (2004). Thermal and mechanical finite element modeling of laser forming from metal and ceramic powders. Acta Materialia, 52, 69-80.

DeHoff, P.H., Anusavice, K.J. (1998). Viscoelastic stress analysis of thermally compatible and incompatible metal-ceramic systems. Dental Materials,14(4),237-45.

Dimitrova, I., Tosheva, D.T. (2023). Comparative analysis of shear bond strength and quality of interface at novel bioactive material or Biodentine. Journal of Ceramic Processing Research, 24(2), 353-358.

Feuerstein, O., Zeichner, K., Imbari, C., Ormianer, Z., Samet, N., Weiss, E.I. (2008). Temperature changes in dental implants following exposure to hot substances in an ex vivo model. Clinical Oral Implants Research,19(6),629-33.

Fischer, J., Stawarzcyk, B., Trottmann, A., Hämmerle, C.H. (2009). Impact of thermal misfit on shear strength of veneering ceramic/zirconia composites. Dental Materials, 25(4),419-23.

Ganesh, I. (2013). A review on magnesium aluminate ($MgAl_2O_4$) spinel: synthesis, processing and applications, International Materials Reviews, 58(2), 63-112.

Guazzato, M., Albakry, M., Swain, M.V., Ironside, J. (2002). Mechanical properties of In-Ceram Alumina and In-Ceram Zirconia. The International Journal of Prosthodontics, 15(4),339-46.

Haskan, H., Boyraz, T., Kilicarslan, M.A. (2007). Investigation of thermal stresses in dental restoration by mathematical method. Journal of European Ceramic Society, 27,899-902.

Hsueh, C.H., Thompson, G.A., Jadaan, O.M., Wereszczak, A.A., Becher, P.F. (2008). Analyses of layer-thickness effects in bilayered dental ceramics subjected to thermal stresses and ring-on-ring tests. Dental Materials, 24(1),9-17.

Hummel, M., Kern, M. (2004). Durability of the resin bond strength to the alumina ceramic Procera. Dental Materials, 20(5),498-508.

Jacobs, H.R., Thompson, R.E., Brown, W.S. (1973). Heat transfer in teeth. J Dent Res, 52, 248-52.

Juntavee, N., Dangsuwan, C. (2018). Role of coefficient of thermal expansion on bond strength of ceramic veneered yttrium-stabilized zirconia. Journal of Clinical and Experimental Dentistry, 10(3), e279-e286.

Kaleli, N, Saraç, D. (2017). Comparison of porcelain bond strength of different metal frameworks prepared by using conventional and recently introduced fabrication methods. Journal of Prosthetic Dentistry,118(1),76-82.

Kanat-Ertürk, B., Çömlekoğlu, E.M., Dündar-Çömlekoğlu, M., Özcan, M., Güngör, M.A. (2015). Effect of Veneering Methods on Zirconia Framework-Veneer Ceramic Adhesion and Fracture Resistance of Single Crowns. Journal of Prosthodontics, 24(8),620-8.

Kern, M., Thompson, V.P. (1995). Bonding to glass infiltrated alumina ceramic: adhesive methods and their durability. Journal of Prosthetic Dentistry, 73(3),240-9.

Khmaj, M.R., Khmaj, A.B., Brantley, W.A., Johnston, W.M., Dasgupta, T. (2014). Comparison of the metal-to-ceramic bond strengths of four noble alloys with press-on-metal and conventional porcelain layering techniques. Journal of Prosthetic Dentistry, 112(5),1194-200.

Kim, B.K., Bae, H.E., Shim, J.S., Lee, K.W. The influence of ceramic surface treatments on the tensile bond strength of composite resin to all-ceramic coping materials. Journal of Prosthetic Dentistry, 94(4),357-62.

Komine, F, Strub, J.R., Matsumura, H. (2012). Bonding between layering materials and zirconia frameworks. Jpn Dent Sci Rev, 48(2),153-161.

Lin, M., Xu, F., Lu, T.J., Bai, B.F. (2010). A review of heat transfer in human tooth-experimental characterization and mathematical modeling. Dental Materials, 26(6), 501-13.

Longhini, D., Rocha, C.O., Medeiros, I.S., Fonseca, R.G., Adabo, G.L. (2016). Effect of Glaze Cooling Rate on Mechanical Properties of Conventional and Pressed Porcelain on Zirconia. Brazilian Dental Journal, 27(5),524-531.

Lopes, S.C., Pagnano, V.O., Rollo, J.M., Leal, M.B., Bezzon, O.L. (2009). Correlation between metal-ceramic bond strength and coefficient of linear thermal expansion difference. Journal of Applied Oral Science,17(2),122-8.

Lubas, M. (2020). Au interface effect on Ti-dental porcelain bond strength investigated by spectroscopic methods and mechanical tests. Journal of Molecular Structure, 1208,127870.

Lunt, A.J.G., Kabra, S., Kelleher, J., Zhang, S.Y., Neo, T.K., Korsunsky, A.M. (2015). Tensile secondary creep rate analysis of a dental veneering porcelain. Thin Solid Films, 596,269-76.

Ma, L., Guess, P.C., Zhang, Y. (2013). Load-bearing properties of minimal-invasive monolithic lithium disilicate and zirconia occlusal onlays: finite element and theoretical analyses. Dental Materials, 29(7),742-51.

Madeira, S., Mesquita-Guimarães, J., Ribeiro, P., Fredel, M., Souza, J.C.M., Soares, D., Silva, F.S., Henriques, B. (2019). Y-TZP/porcelain graded dental restorations design for improved damping behavior - A study on damping capacity and dynamic Young's modulus. Journal of the Mechanical Behavior of Biomedical Materials, 96,219-226.

Neto, A.J.F., Panzeri, H., Neves, F.D., Prado, R.A., Mendonça, G. (2006). Bond strength of three dental porcelains to Ni-Cr and Co-Cr-Ti alloys. Brazilian Dental Journal,17(1),24-8.

Rezaie, H. R., et al., (2020). A Review on Dental Materials. Springer Nature.

Rynıewıcz, W., Rynıewıcz, A.M., Bojko, L., Mazur, K. (2020). The Simulation Assessment of The Veneering Layers of Prosthetic Crowns İn Concentrated Contact, Tribologia, 293(5), 39-50.

Saito, A., Komine, F., Blatz, M.B., Matsumura, H. (2010). A comparison of bond strength of layered veneering porcelains to zirconia and metal. Journal of Prosthetic Dentistry,104(4),247-57.

Sendão, I.A., Alves, A.C., Galo, R., Toptan, F., Silva, F.S., Ariza, E. (2015). The effect of thermal cycling on the shear bond strength of porcelain/Ti-6Al-4V interfaces. Journal of the Mechanical Behavior of Biomedical Materials, 44,156-63.

Suansuwan, N., Swain, M.V. (2001). Determination of elastic properties of metal alloys and dental porcelains. Journal of Oral Rehabilitation, 28(2),133-9.

Tribst, J.P.M., Lo Giudice, R., Dos Santos, A.F.C., Borges, A.L.S., Silva-Concílio, L.R., Amaral, M., Lo Giudice, G. (2021). Lithium Disilicate Ceramic Endocrown Biomechanical Response According to Different Pulp Chamber Extension Angles and Filling Materials. Materials (Basel), 14(5),1307.

Trindade, F.Z., Valandro, L.F., de Jager, N., Bottino, M.A., Kleverlaan, C.J. (2018). Elastic Properties of Lithium Disilicate Versus Feldspathic Inlays: Effect on the Bonding by 3D Finite Element Analysis. Journal of Prosthodontics, 27(8),741-747.

Toptan, F., Alves, A.C., Henriques, B., Souza, J.C., Coelho. R., Silva, F.S., Rocha, L.A., Ariza, E. (2013). Influence of the processing route of porcelain/Ti-6Al-4V interfaces on shear bond strength. Journal of the Mechanical Behavior of Biomedical Materials, 20,327-37.

Valandro, L.F., Ozcan, M., Bottino, M.C., Bottino, M.A., Scotti, R., Bona, A.D. (2006). Bond strength of a resin cement to high-alumina and zirconia-reinforced ceramics: the effect of surface conditioning. The Journal of Adhesive Dentistry, 8(3),175-81.

Vojdani, M., Shaghaghian, S., Khaledi, A., Adibi, S. (2012). The effect of thermal and mechanical cycling on bond strength of a ceramic to nickel-chromium (Ni-Cr) and cobalt-chromium (Co-Cr) alloys. Indian Journal of Dental Research, 23,509-513.

Vásquez, V.Z., Ozcan, M., Kimpara, E.T. (2009). Evaluation of interface characterization and adhesion of glass ceramics to commercially pure titanium and gold alloy after thermal- and mechanical-loading. Dental Materials, 25(2),221-31.

Wang, H., Lim, J.Y. (2019). Metal-ceramic bond strength of a cobalt chromium alloy for dental prosthetic restorations with a porous structure using metal 3D printing. Computers in Biology and Medicine | Journal, 112,103364.

Warreth, A., Elkareimi, Y. (2020). All-ceramic restorations: A review of the literature. The Saudi Dental Journal, 32(8),365-372.

Weber, K.R., Benetti, P., Della Bona, Á., Corazza, P.H., Medeiros, J.A., Lodi, E., Borba, M. (2018). How does the piston material affect the in vitro mechanical behavior of dental ceramics? Journal of Prosthetic Dentistry, 120(5),747-754.

Wiedenmann, F., Klören, M., Edelhoff, D., Stawarczyk, B. (2021). Bond strength of CAD-CAM and conventional veneering materials to different frameworks. Journal of Prosthetic Dentistry, 125(4),664-673.

Wood, D.J., Bubb, N.L., Millar, B.J., Dunne, S.M. (1997). Preliminary investigation of a novel retentive system for hydrofluoric acid etch-resistant dental ceramics. Journal of Prosthetic Dentistry, 78(3), 275-80.

Wood, D.J., Shiraishi, T., Shinozaki, N., van Noort, R. (2008). Spectral reflectance and color of dentin ceramics for all-ceramic restorations. Dental Materials, 24(12),1661-9.

Yadav, R., Kumar, M. (2019). Dental restorative composite materials: A review. Journal of Oral Biosciences, 61(2),78-83.

Yoshimura, H.N., Gonzaga, C.C., Cesar, P.F., Miranda, W.G Jr. (2012). Relationship between elastic and mechanical properties of dental ceramics and their index of brittleness. Ceramic International, 38(6),4715-22.

Zhang, Z., Tan, F., Ba, Y., Zhang, Y. (2013). Effects of different bond agents on commercially pure Ti-porcelain bond strength. Mater Letters, 109,214-216.

Zinelis, S., Barmpagadaki, X., Vergos, V., Chakmakchi, M., Eliades, G. (2010). Bond strength and interfacial characterization of eight low fusing porcelains to cp Ti. Dental Materials, 26(3),264-73.